

This is the accepted manuscript made available via CHORUS, the article has been published as:

One-dimensional itinerant interacting non-Abelian anyons

Didier Poilblanc, Adrian Feiguin, Matthias Troyer, Eddy Ardonne, and Parsa Bonderson

Phys. Rev. B **87**, 085106 — Published 6 February 2013

DOI: [10.1103/PhysRevB.87.085106](https://doi.org/10.1103/PhysRevB.87.085106)

One-dimensional itinerant interacting non-Abelian anyons

Didier Poilblanc,^{1,*} Adrian Feiguin,² Matthias Troyer,³ Eddy Ardonne,^{4,5} and Parsa Bonderson⁶

¹*Laboratoire de Physique Théorique UMR-5152, CNRS and Université de Toulouse, F-31062 France*

²*Department of Physics, Northeastern University, Boston, Massachusetts 02115, USA*

³*Theoretische Physik, ETH Zurich, 8093 Zurich, Switzerland*

⁴*Nordita, Royal Institute of Technology and Stockholm University,
Roslagstullsbacken 23, SE-106 91 Stockholm, Sweden*

⁵*Department of Physics, Stockholm University, AlbaNova University Center, SE-106 91 Stockholm, Sweden*

⁶*Station Q, Microsoft Research, Santa Barbara, California 93106-6105, USA*

(Dated: January 18, 2013)

We construct models of interacting itinerant non-Abelian anyons moving along one-dimensional chains. We focus on itinerant Ising (Majorana) and Fibonacci anyons, which are, respectively, related to $SU(2)_2$ and $SU(2)_3$ anyons and also, respectively, describe quasiparticles of the Moore-Read and \mathbb{Z}_3 -Read-Rezayi fractional quantum Hall states. Following the derivation of the electronic large- U effective Hubbard model, we derive effective anyonic t - J models for the low-energy sectors. Solving these models by exact diagonalization, we find a fractionalization of the anyons into charge and (neutral) anyonic degrees of freedom – a generalization of spin-charge separation of electrons which occurs in Luttinger liquids. A detailed description of the excitation spectrum can be performed by combining spectra for charge and anyonic sectors. The anyonic sector is the one of a *squeezed* chain of localized interacting anyons, and hence is described by the same conformal field theory (CFT), with central charge $c = 1/2$ for Ising anyons and $c = 7/10$ or $c = 4/5$ for Fibonacci anyons with antiferromagnetic or ferromagnetic coupling, respectively. The charge sector is the spectrum of a chain of hardcore bosons subject to phase shifts which coincide with the momenta of the combined anyonic eigenstates, revealing a subtle coupling between charge and anyonic excitations at the microscopic level (which we also find to be present in Luttinger liquids), despite the macroscopic fractionalization. The combined central charge extracted from the entanglement entropy between segments of the chain is shown to be $1 + c$, where c is the central charge of the underlying CFT of the localized anyon (squeezed) chain.

PACS numbers: 75.10.Kt, 75.10.Jm, 75.40.Mg

I. INTRODUCTION

One of the most significant pursuits in condensed matter physics is the search for quasiparticles or excitations that obey non-Abelian exchange statistics^{1–4}. The most prominent candidates (at present) are excitations of non-Abelian quantum Hall states^{5–9}. In particular, there is evidence from tunneling¹⁰ and interferometry^{11,12} experiments supporting the existence of non-Abelian quasiparticle excitations for the $\nu = 5/2$ quantum Hall state^{13–15}.

The leading candidate quantum Hall states to describe the electronic ground state of the quantum Hall plateau at filling fraction $\nu = 5/2$ are the Moore-Read (MR) Pfaffian state⁵ or its particle-hole conjugate, the “anti-Pfaffian” (aPf) state^{7,8}. Despite the differences between the MR and aPf states (which manifest in the detailed structure of the edge states), the non-Abelian anyonic structure of their bulk quasiparticles are simply the complex conjugates of each other. Both can be described in terms of an Ising-type anyon model.

One of the leading candidates to describe the experimentally observed $\nu = 12/5$ quantum Hall plateau^{16,17} is the $k = 3$ Read-Rezayi (RR) state⁶ (a generalization of the MR state), or, more precisely, its particle-hole conjugate (\overline{RR}). The non-Abelian quasiparticles of the RR and \overline{RR} states are of Fibonacci type, and the $\nu = 12/5$ quantum Hall state is the leading candidate system host-

ing such non-Abelian anyons. The other leading candidate for describing the $\nu = 12/5$ quantum Hall effect is provided by Bonderson-Slingerland (BS) states⁹ obtained hierarchically from the MR and aPf $\nu = 5/2$ states (by condensing Laughlin-type quasiholes). The quasiparticles of these BS states have a similar Ising-type non-Abelian structure as their MR and aPf parent states. Numerical studies of the $\nu = 12/5$ quantum Hall state found the \overline{RR} and BS candidates to be in close competition¹⁸.

Interestingly, a different hierarchical construction over the MR state (condensing fundamental non-Abelian quasielectrons) produces a candidate state for filling $\nu = 18/7$ that possesses non-Abelian quasiparticles of the Fibonacci type¹⁹, similar to the ones appearing in the non-Abelian spin-singlet (NASS) state²⁰. However, a quantum Hall state at $\nu = 18/7$ has, so far, not been experimentally observed.

Another promising class of candidates for realizing non-Abelian quasiparticles is provided by systems with the so-called emergent Majorana zero modes, which behave like Ising-type anyons under exchange. Majorana zero modes were originally predicted to exist in vortex cores of chiral p-wave superconductors^{21,22} or at the ends of one-dimensional polarized superconductors²³. More recently, it was shown that Majorana fermions can form at the interface of a strong topological insulator and an

s-wave superconductor²⁴. This idea for realizing Majorana fermion zero modes was further developed by several groups^{25–28}, who proposed similar superconducting heterostructures based on semiconductors exhibiting strong spin-orbit coupling, rather than topological insulators. For a review, see Ref. 29. Efforts to physically implement these latest proposals have been made in recent experiments^{30–33} consisting of electrons tunneling into a nanowire (set-up to be in a topological phase supporting edge Majorana modes). However, neither the exponential localization to the edges of the observed zero-modes nor the non-Abelian exchange statistics has been probed yet.

Inspired by these recent developments and possible realizations of quasiparticles with non-Abelian statistics, we consider the question of what happens if one confines mobile non-Abelian quasiparticles to one-dimensional (1D) systems. The concept of itinerancy of interacting non-Abelian quasiparticles is of direct physical significance, and the microscopic models we study can be viewed, for example, as (crude) effective models relevant to edge modes of quantum Hall and Majorana fermion systems. It was established long ago, starting with the work of Anderson³⁴, that electrons confined to one dimension undergo “spin-charge separation,” namely the electrons falls apart into two pieces, one spinless carrying the charge, the other a spinon without charge, carrying the spin. These ideas were further developed by several people, Tomonaga³⁵, Luttinger³⁶, and Haldane³⁷, who introduced the concept of the one-dimensional *Luttinger liquid*.

In our recent Letter³⁸, we started to investigate the subject of itinerant non-Abelian anyons in a one-dimensional system. We established that non-Abelian anyons (of which the quasiparticles of the quantum Hall states and the Majorana zero modes discussed above are prime examples) also undergo a process which resembles spin-charge separation. Namely, the non-Abelian anyons fractionalize into charge (or density) and anyonic degrees of freedom. The model introduced in Ref. 38 was inspired by the electronic t - J model³⁹, which can be viewed as a limiting case of the Hubbard model^{40–42} – namely in the limit of large on-site repulsion – and for which spin-charge separation was established analytically at a supersymmetric point^{43–45} and numerically⁴⁶. In this paper, we continue our study of itinerant non-Abelian anyons and provide greater detail.

The outline of the paper is as follows: in Sec. II we review briefly general properties of non-Abelian anyons in $SU(2)_k$ Chern-Simons theories and, more specifically, in non-Abelian quantum Hall states. In Sec. III, we show that, in close analogy to the electronic case, it is possible to: (i) truncate the Hilbert space of the quasiparticles of the non-Abelian quantum Hall states confined to a one-dimensional geometry (in the case of strong charging energy), and (ii) derive low-energy effective anyonic t - J models. The charge sectors of the anyonic t - J models are derived in Sec. IV. In Sec. V, we present a short

review of the properties of dense (localized) non-Abelian anyon chains. In Sec. VI, we demonstrate that the excitation spectrum of the anyonic t - J models can be accurately described by combining spectra for charge and anyonic sectors (in a subtle manner), and provide clear evidence of the fractionalization of anyons into charge and anyonic degrees of freedom. In Sec. VII, we use density matrix renormalization group (DMRG) calculations to extract the central charge of the Fibonacci t - J chain from the entanglement entropy between segments of open chains, providing further evidence of fractionalization. In Appendix A, we provide detailed descriptions of the related anyon models of the MR and RR states. In Appendix B, we describe the details of the quasiparticle spectrum truncation for MR and RR anyons used in the paper.

II. NON-ABELIAN ANYONS

A. General considerations and fusion algebra

The non-Abelian anyons we will be concerned with in this paper can formally be described by $SU(2)_k$ Chern-Simons theories, or via a certain quantum deformation of $SU(2)$. In either case, the non-Abelian degrees of freedom are captured by the “topological charges” j , which can be thought of as “generalized angular momenta.” For a given $SU(2)_k$ theory, these are constrained to take the values $j = 0, \frac{1}{2}, \dots, \frac{k}{2}$, loosely corresponding to the first $k+1$ representations of $SU(2)$.

In the same way that the tensor product of $SU(2)$ spins can be decomposed into the direct sum of multiplets of definite values of J^2 , one can decompose the product, or “fusion” of anyons. This fusion algebra or “fusion rules” of a general anyon model takes the form

$$a \times b = \sum_{c \in \mathcal{C}} N_{ab}^c c \quad (1)$$

where a , b , and c are topological charge values in the set of allowed topological charges \mathcal{C} , and the fusion coefficients N_{ab}^c are non-negative integers indicating the number of ways a and b can fuse to produce c . The N_{ab}^c must be such that the algebra is commutative and associative. There must also be a unique “vacuum” or “trivial” charge, which we denote as I or 0 , for which $N_{a0}^c = \delta_{ac}$.

The fusion rules of $SU(2)_k$ anyons resemble their $SU(2)$ counterpart (but with a finite set of allowed values for j and a corresponding truncation of the algebra). In particular

$$j_1 \times j_2 = \sum_{j_3=|j_1-j_2|}^{\min\{j_1+j_2, k-j_1-j_2\}} j_3, \quad (2)$$

where the upper limit is such that the fusion rules are associative and obey the constraint that $j_i \leq \frac{k}{2}$.

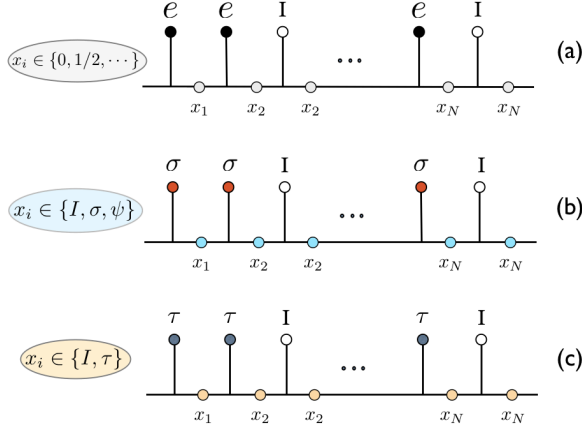


FIG. 1: Anyonic fusion trees for (a) electrons, (b) Ising σ anyons, and (c) Fibonacci anyons. Sites are denoted by the (filled or empty) circles at top of the diagrams. Empty circles denote vacant sites, which carry the vacuum or trivial topological charge 0 or I . The bond labels $\{x_i\}$ encode non-local information about the state and their possible values are specified for each model. We note that, for Ising anyons, our model excludes ψ anyons on the sites, but not on the links (see the main text).

We will be particularly interested in the cases $k = 2$ and 3, because they are the experimentally most relevant non-Abelian anyon models. (The case $k = 1$ corresponds to Abelian anyon models, in which case the Hilbert spaces we construct below are one-dimensional, so one can not construct non-trivial models.) These cases are related to the Ising and Fibonacci anyons models, respectively, which we now consider in more detail.

The anyon model with $k = 2$ has three anyon types, which we will label using the Ising TQFT topological charges I , σ , and ψ as follows: The vacuum or trivial anyon I corresponds to $j = 0$. The anyon of type σ corresponds to $j = \frac{1}{2}$. Finally, the (fermionic) anyon type ψ corresponds to $j = 1$. In particular, the fusion rules read⁸³

$$\sigma \times \sigma = I + \psi \quad \sigma \times \psi = \sigma \quad \psi \times \psi = I, \quad (3)$$

in addition to the general relations $\alpha \times \beta = \beta \times \alpha$ and $I \times \alpha = \alpha$, which hold in all anyon models, for arbitrary α and β .

The Fibonacci anyon model correspond to the case $k = 3$, where we restrict ourselves to the integer-valued $j = 0$ and 1, which we will label as the vacuum I and the Fibonacci anyon τ , respectively.⁸⁴ The Fibonacci fusion rule reads

$$\tau \times \tau = I + \tau. \quad (4)$$

In the following we shall consider itinerant anyons moving on one dimensional chains. Pictorial representations of such anyonic chains are shown in Fig. 1(b,c), together with the more familiar case of strongly correlated electrons shown in Fig. 1(a).

For the case of strongly correlated electrons, each electron carries a unit charge and spin- $\frac{1}{2}$. The spin- $\frac{1}{2}$ degrees of freedom are taken into account in Fig. 1(a) in a slightly unconventional way, utilizing a “fusion tree” notation, rather than the usual tensor product of N two-dimensional local Hilbert spaces (where N is the number of electrons). In this notation, the labels x_i for the links of the fusion tree correspond to the total spin obtained by combining the spin x_{i-1} with that of the i th electron. For an open chain, this simply means that x_i is the total spin of all the electrons to the left of the label. For a periodic chain (in a system on a torus), the label has a slightly more abstract interpretation, since the notion of all particles to the left or right are not well-defined. We use this formulation because it easily generalizes to the case of non-Abelian anyons, where there are no local degrees of freedom (i.e. they lack local Hilbert spaces and internal quantum numbers, similar to s_z in the case of spins).

The non-Abelian anyons in Fig. 1(b,c) may also carry electric charge (albeit this typically is a fraction of the charge of the electron), as well as anyonic degrees of freedom. The charge degrees of freedom live on the sites, while the bond variables x_i encode the anyonic degrees of freedom along the fusion tree, in the same way as the labels x_i encoded the spin of the electrons in Fig. 1(a). Abelian anyonic degrees of freedom may be treated in the same way as electric charge, i.e. locally assigned to the sites, since their resulting fusion tree is uniquely determined by the local degrees of freedom. The labels x_i are not arbitrary, but satisfy the constraint that each trivalent vertex in this fusion tree is permitted by the fusion rules. This implies that the size of the *internal* Hilbert space (for a given configuration of particle/anyon positions) grows as 2^N in the case of the electrons, $(\sqrt{2})^N$ in the case of the Ising anyons, and ϕ^N in the case of the Fibonacci anyons, where $\phi = \frac{1+\sqrt{5}}{2}$ is the golden ratio. Here, N corresponds to the number of electrons, Ising σ anyons, or Fibonacci anyons. The actual dimension for any finite N is, of course, an integer, so these are only the leading order scaling (as $N \rightarrow \infty$) for the non-Abelian anyons. The sites labeled by I correspond to vacancies, and carry no electric charge, spin, or anyonic degrees of freedom.

Before we continue in the next subsection with describing the quantum Hall states in which these types of anyons are realized, we want to make one remark, which will be essential in the subsequent description of the behavior of the itinerant anyons. Despite the fact that we will be describing mobile, but identical, anyons, there will be a notion of “distinguishability” of the anyons. In particular, the various states in the Hilbert space are not only characterized by the location of the occupied sites, but also by the labels x_i , which distinguish the various states, given the location of all the anyons. In some sense, specifying the precise internal state, corresponding to all the anyons as a whole, renders the individual anyons in a particular state distinguishable. We will see later on that

this seemingly simple observation will play an essential role in the effective description of the collective behavior of the itinerant anyons.

B. Non-Abelian quantum Hall states

We now concentrate on describing the anyonic structure of the MR and $k = 3$ RR states in their fermionic incarnations, which are relevant in the electronic quantum Hall setting. Because of the fermionic nature of the states, the anyonic structure is slightly more complicated than the $SU(2)_k$ anyons described above. To describe this structure, it is best to consider the non-Abelian part separately, which is described in terms of Ising anyons for the MR state, and \mathbb{Z}_3 parafermions for the $k = 3$ RR state.

In the case of the MR state, the non-Abelian sector is the Ising theory, whose fields are I, σ, ψ , with the Ising fusion rules given above. The quasiparticle types can now be specified by the Ising label, together with the electric charge. The vacuum is $(I, 0)$, while $(\sigma, e/4)$ is the “fundamental quasiparticle,” which, in some sense, carries the “smallest” quantum numbers allowed in the MR state, i.e. it has the smallest (nonzero) electric charge and repeated fusion generates the entire spectrum of topological charges. All other quasiparticles are thus obtained by repeated fusion of this fundamental quasiparticle, using the fusion rules above and the additivity of the charge. In addition, one needs the rule that quasiparticles which differ by fusion of an electron, given by (ψ, e) are to be identified. The fact that we identify quasiparticles which “differ by a fermion” (or identify the electron with the vacuum) leads to some complications, which are not present for the bosonic versions of these quantum Hall states⁸⁵, but these complications will not concern us here. The resulting quasiparticle spectrum is given in Fig. 2(b), where we have six different quasiparticle types (shown as green circles), because (I, e) and $(\psi, 0)$ are identified, and so on.

In the case of the RR state with $k = 3$, the non-Abelian structure corresponds to the \mathbb{Z}_3 -parafermions, which conventionally are labeled as $I, \psi_1, \psi_2, \sigma_1, \sigma_2, \varepsilon$. We will, however, use the notation $\psi_0 = I, \tau_0 = \varepsilon, \tau_2 = \sigma_1$ and $\tau_1 = \sigma_2$. In this way, the fusion rules take the simple form

$$\begin{aligned} \psi_i \times \psi_j &= \psi_{i+j} \\ \psi_i \times \tau_j &= \tau_{i+j} \\ \tau_i \times \tau_j &= \psi_{i+j} + \tau_{i+j}, \end{aligned} \quad (5)$$

where the indices are taken modulo 3. This is the direct product of the Fibonacci fusion algebra with a \mathbb{Z}_3 fusion algebra. The quasiparticle types can now be specified by the \mathbb{Z}_3 -parafermion label, together with the electric charge. The vacuum is $(\psi_0, 0)$ while the fundamental quasiparticle’s quantum numbers are $(\tau_2, e/5)$. As in the MR state, the other quasiparticles are obtained by repeated fusion of the fundamental quasiparticle, using the

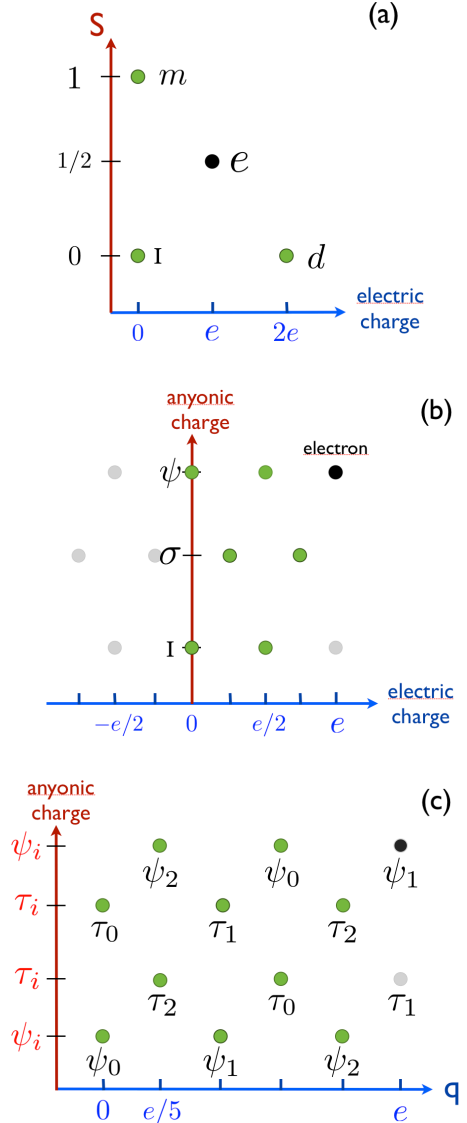


FIG. 2: Charts of the quasiparticle contents of (a) the electronic Hubbard model, (b) the MR state and (c) the $k = 3$ RR state. The elementary electric charges of the MR quasiparticles are multiples of $e/4$, while that of the RR quasiparticles are multiples of $e/5$. The dark (green) symbols correspond to the different particle types. The black dots represent electrons/holes, which are identified with the vacuum $(I, 0)$ in (b) and the vacuum $(\psi_0, 0)$ in (c). The grey dots correspond to particles which are identified with one of the particles corresponding to a green symbol, as explained in the main text.

fusion rules above. Quasiparticles which differ by fusion of an electron, given by (ψ_1, e) , are to be identified. This gives rise to ten different quasiparticle types displayed as green circles in Fig. 2(c), with charges $0, \dots, 4e/5$ [where we note that (τ_1, e) is identified with $(\tau_0, 0)$, and so on].

For comparison, we display the relevant quasiparticle types in the ordinary electron case in Fig. 2(a): the trivial particle (vacant site) I , the electron e , a double occupied

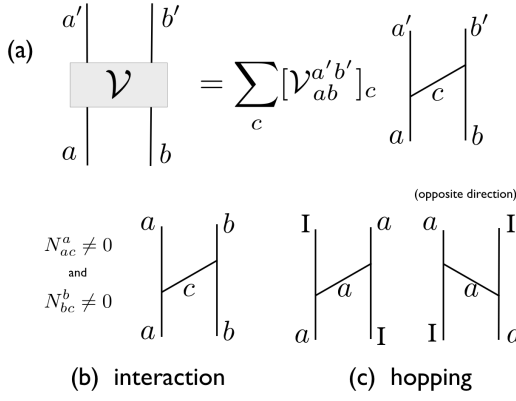


FIG. 3: (a) All two-anyon processes can be represented as a general “tunneling” term, where topological (and/or electrical) charge is transferred from one localized quasiparticle to the other. Special cases of this include (b) an “interaction” between the two anyons, for which the localized charges are unchanged, and (c) a “hopping” term, where a localized anyon moves to a vacant site.

site d and a spin-1 magnon m . In this case, there is no condensate, and hence none of the particles are to be identified.

In the next section, we will describe how we can truncate the spectrum of particles, in order to come up with a tractable model of interacting, itinerant anyons in one dimension.

III. ANYONIC t - J MODELS

A. Objectives and procedure

We move now to the construction of the low energy models for the itinerant anyons in one dimension, modeled by a discrete chain. This chain might be a lattice discretization of a one-dimensional continuum system such as the edge of a quantum Hall liquid or a one-dimensional array of quantum dots. On this chain we restrict ourselves to short-range (nearest-neighbor) interactions and “hopping” terms that can both be expressed as “tunneling” processes⁴⁷, as sketched in Figs. 3,4. Because the anyons are electrically charged, confinement on a quantum dot or transverse confinement (e.g. in the case of edge states) may lead to large Coulombic charging energy that strongly discourages multiple occupancy of sites and, hence, prohibits the formation of quasiparticle excitations of larger charge values.

As seen in the previous section the physical contents of the non-Abelian quantum Hall states are very rich and we thus want to derive an effective low-energy model, similar to the derivation of the t - J model for electrons from the Hubbard model. In order to describe the low-energy spectra, a well-know strategy consists of building up a simpler model by (i) discarding the high-energy (quasi)particles and (ii) treating virtual processes involv-

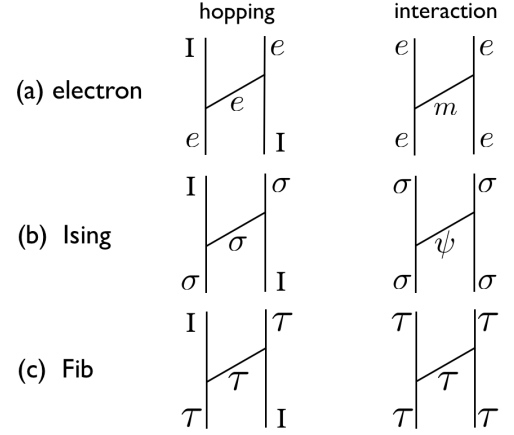


FIG. 4: Hopping and interaction terms for (a) electrons, (b) Ising anyons, and (c) Fibonacci anyons, expressed in the notations of Fig. 3.

ing the fusion of the low-energy (quasi)particles to the discarded high-energy (quasi)particles in second-order perturbation theory.

B. Large- U electronic Hubbard model

To illustrate this procedure, we first take the example of a generalized Hubbard model of electrons and show how to derive the corresponding t - J model. We start from electrons, where the most general $SU(2)$ -symmetric single band model with nearest neighbor interactions can be written in second quantized notation as

$$\begin{aligned}
 H = & -t \sum_{i,\sigma} \left(c_{i,\sigma}^\dagger c_{i+1,\sigma} + H.c. \right) \\
 & + J_0 \sum_i \left(\vec{S}_i \cdot \vec{S}_{i+1} - \frac{1}{4} n_i n_{i+1} \right) \\
 & + V \sum_i n_i n_{i+1} \\
 & + U \sum_i n_{i,\uparrow} n_{i,\downarrow}.
 \end{aligned} \tag{6}$$

Here $c_{i,\sigma}^\dagger$ and $c_{i,\sigma}$ are the creation and annihilation operators of an electron with z -component of spin σ , $n_{i,\sigma} = c_{i,\sigma}^\dagger c_{i,\sigma}$ are the local spin densities, $n_i = n_{i,\uparrow} + n_{i,\downarrow}$ is the total local density, and \vec{S}_i is the spin operator on site i .

The first term (t) in the Hamiltonian of Eq. (6) is the hopping (tunneling) of an electron. The second term (J_0) is a spin exchange term, which can be interpreted as a two-electron interaction mediated by the tunneling of a spin-1 magnon. This term can also be written as $-J \mathcal{P}_{i,i+1}^{S=0}$, with $\mathcal{P}_{i,i+1}^{S=0}$ being the projector onto the total singlet state of two neighboring electrons at sites i and $i+1$. The third term (V) is a nearest neighbor repulsion, which can be interpreted as tunneling of a photon, and finally the last term (U) is the local charging energy.

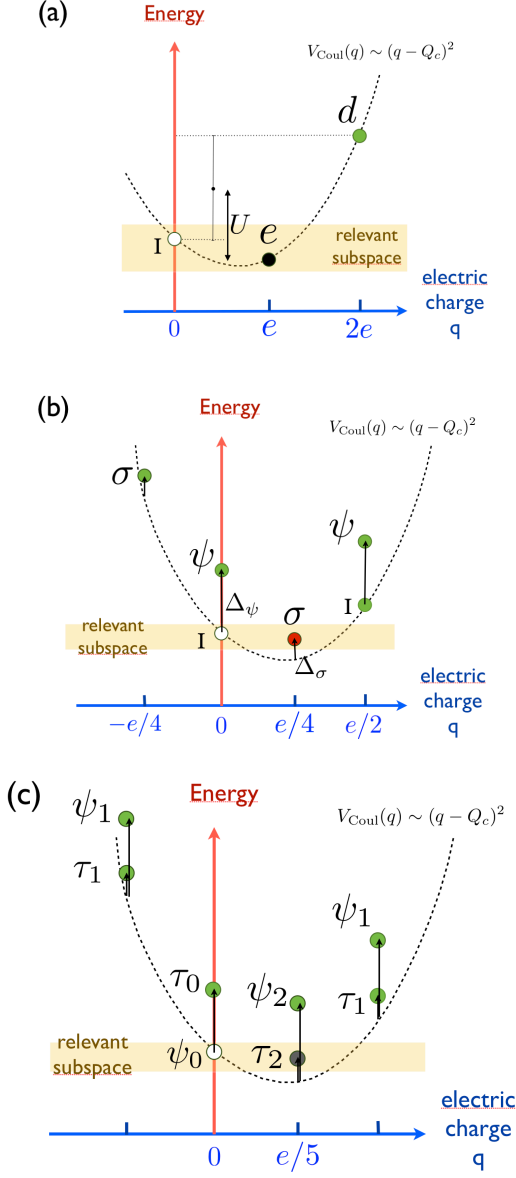


FIG. 5: Schematic energy spectra (arbitrary scale) in the presence of a parabolic Coulomb charging energy for the case of (a) electrons, (b) Ising anyons, and (c) Fibonacci anyons. The Hubbard U energy is shown in (a). Upward arrows show the shifts corresponding to the topological contribution to the bare energies of the quasiparticles, e.g. $\Delta_\sigma = 1/8$ and $\Delta_\psi = 1$ in (b), $\Delta_{\tau_0} = 4/5$, $\Delta_{\tau_1} = \Delta_{\tau_2} = 2/15$ and $\Delta_{\psi_1} = \Delta_{\psi_2} = 4/3$ in (c).

In this Hubbard model of electrons, we consider three different types of “quasiparticles” at the lowest energies: the “trivial particle” I (i.e. a vacant site), the electron e , and the “doublon” d , corresponding to a double (electronic) occupancy on a site. In Fig. 5(a), we model the energy costs for a given quasiparticle type using a parabolic Coulombic charging energy of the form

$$V_{\text{Coul}}(q) \sim (q - Q_c)^2 \quad (7)$$

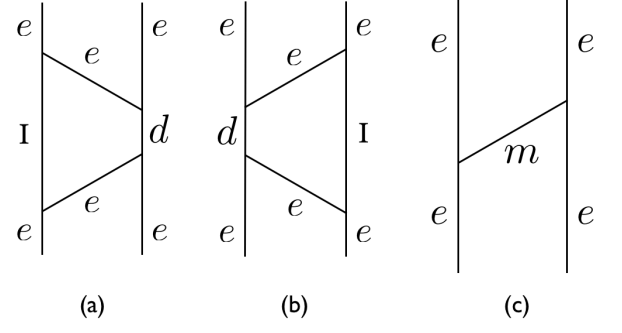


FIG. 6: (a,b) Second-order exchange processes for two electrons on nearest neighbor sites via the virtual creation of a “vacuum” quasiparticle I (i.e. a vacancy) and a “doublon” d . These two exchange diagrams can be replaced by a first-order magnon exchange diagram, shown in (c), leading to a renormalization of the magnon exchange interaction.

where q is the quasiparticle’s electric charge value, and Q_c is the minimal energy charge value. Here, each lattice site is viewed as a “quantum dot” for which Q_c is fixed by the (implicit) chemical potential. The last term in the Hamiltonian of Eq. (6) specifies that U is the energy cost for promoting two electrons into a vacancy and a doublon. When U/t is large, one can project out doublons and consider a restricted subspace of electrons and vacancies only. The local U interaction can then be taken into account in second-order perturbation, as shown in Fig. 6, renormalizing the coupling constant of the spin exchange term to $J = J_0 + 4t^2/U$, i.e. the magnon mediated interaction.

C. Hilbert space truncation for anyons

For anyons we proceed in the same way as for the electronic Hubbard model to derive a simpler effective model of the low lying states, assuming that the charging energy is the largest energy scale and can be integrated out. In Figs. 5(b,c), we model the energy costs for a given quasiparticle type using a quantum dot, which again has a quadratic Coulombic charging energy $V_{\text{Coul}}(q)$, but also has an energy shift

$$V_{\text{neut}}(a) \propto \Delta_a, \quad (8)$$

where Δ_a is the conformal scaling dimension corresponding to topological charge a , which depends on the (neutral) topological charge of the quasiparticle⁴⁸ (see also Refs. 49–52). We note that conformal scaling dimension Δ_a is the sum of the left and right conformal weights $\Delta_a = h_a + \bar{h}_a$.

For large charging energy we can restrict ourselves to a low-energy subspace that contains only two quasiparticle types, as indicated in Figs. 5(b,c). In the case of the Ising anyon chain, we only allow the lowest energy quasiparticles ($I, 0$) and $(\sigma, e/4)$ to be localized on a given site. The

quasiparticles $(I, e/2)$ and $(\psi, e/2)$ correspond physically to double occupancies of the quasiparticle $(\sigma, e/4)$, and thus involve a prohibitively large Hubbard-like charging energy. The neutral fermion quasiparticle $(\psi, 0)$ is gapped, because of the energy associated with the ψ mode, but it will be present in our model in the form of virtual tunneling processes. To make the quasiparticles $(I, 0)$ and $(\sigma, e/4)$ nearly degenerate, one has to introduce a chemical potential, which combined with the charging energy gives the sought after near-degeneracy. Similarly, in the case of Fibonacci anyons, we can also allow only the lowest energy quasiparticles $(\psi_0, 0)$ and $(\tau_2, e/5)$ to be localized on a given site. In this case, the neutral Fibonacci quasiparticle $(\tau_0, 0)$ is gapped, but will be present in our model in the form of virtual tunneling processes. In Appendix B, we explain in more detail how one can combine the effects of a gate and of the charging energy in order to obtain a low-energy sector containing two degenerate states, separated from the other excitations by a gap.

We note that the fundamental quasiparticles of the MR or RR quantum Hall states are described as a product of an Ising or Fib anyon model with an Abelian anyon model (see Appendix A) which can be associated to the electric charge and is, therefore, “additive.” Hence, the electric charges of the quasiparticles of the relevant subspace need not to be specified any more, because each quasiparticle has the same charge. Also, we can drop the subscripts for the two lowest-energy Fibonacci quasiparticles, i.e. we identify $\psi_0 \rightarrow I$ and $\tau_2 \rightarrow \tau$ since only one species of τ -anyons is involved in the low-energy subspace. In other words, we end up with only one type of σ -anyon or τ -anyon allowed on the sites and the sites left empty are filled with trivial quasiparticles I or vacancies. The details of the above mentioned identification are not important here, but will be given in Appendix B.

A pictorial representation of such chains was shown in Fig. 1. The charge degrees of freedom can therefore be thought of as living on the sites (the localized nontrivial quasiparticles carry elementary $e/4$ or $e/5$ electric charge, in contrast to the vacancies) while the bond variables x_i are encoding the anyonic (or spin) degrees of freedom. We recall that $a \times I = a$ for any quasiparticle $a = I, \tau, \sigma, \psi$ so that the anyonic “spin” is conserved along the empty segments of the chain (i.e. with vacancies on the sites).

D. Interaction between nearest-neighbor anyons

Let us consider putting N anyons of type σ or τ on an L -site chain with periodic boundary conditions (PBC), i.e. on a closed ring (situated on a torus). When two charged anyons sit on nearest-neighbor (NN) sites they experience an ordinary Coulomb repulsion V . In addition, they interact via an effective exchange interaction of magnitude J , which can be derived as in the electronic Hubbard chain. For this, we use the (unitary) F -symbol transformation shown in Fig. 7, which is a change of ba-

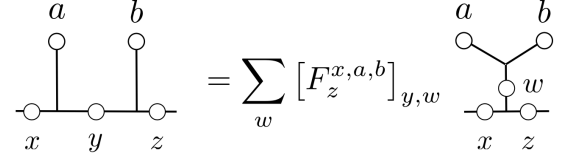


FIG. 7: Change of basis involving the fusion channel of two neighboring electrons or anyons and the F -symbol.

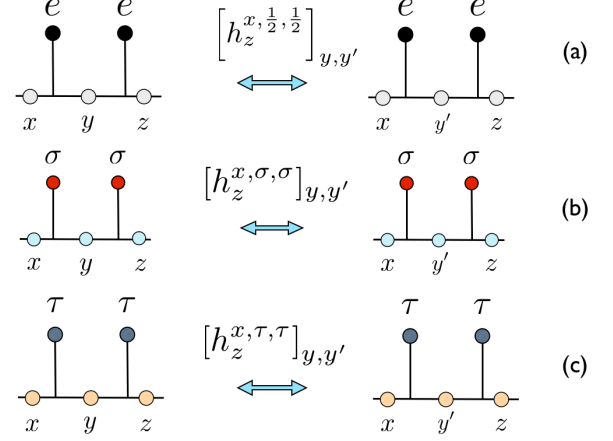


FIG. 8: Matrix elements describing (exchange) interactions between nearest neighbors of (a) electrons, (b) Ising anyons, and (c) Fibonacci anyons. In (b), when $x = z = \sigma$, y and y' can take the values I or ψ , making $h_z^{\sigma, \sigma, \sigma}$ a 2×2 matrix, while when neither x nor z equals σ , then $y = y' = \sigma$, making $h_z^{x, \sigma, \sigma}$ a 1×1 matrix.

sis between different fusion tree representations of the states. When we apply the F -symbol of the NN anyons, which have charges a and b , it provides a change of basis from the fusion chain basis of Fig. 1 (which we use to encode states) to one in which the fusion channel of this NN pair of anyons is manifest, as indicated in Fig. 7 by the charge label w .

By analogy with the electronic Heisenberg interaction, the exchange interaction between two neighboring anyons is given by $-J\mathcal{P}^I$, which favors the vacuum fusion channel I for these two anyons. The action of the corresponding exchange processes on the local fusion tree basis elements are shown schematically in Figs. 8(a-c). By using the F -symbol change of basis of Fig. 7, the local Hamiltonian elements $h_{x_{i+1}}^{x_{i-1}, \alpha_i, \alpha_{i+1}}$ can be derived, depending on (and labelled by) the variables x_{i-1} and x_{i+1} on the two outer bonds connected to the two NN sites and acting upon the local spin x_i of the inner bond, as shown in Fig. 8(a-c). The label α_i denotes the type of anyon localized at site i . Severe local constraints greatly reduce the number of possible non-zero matrices and matrix elements, which we give explicitly below.

Let us first start with the case of two NN spin-1/2 (localized) electrons experiencing an AF exchange interaction, i.e. for which the fusion outcome in the singlet chan-

nel is favored over the triplet channel. In the usual spin-basis, this is just the Heisenberg term $-J(1/4 - \mathbf{S}_i \cdot \mathbf{S}_{i+1})$. However, we work in the fusion chain basis, as pictured in Fig. 1(a). Thus, we need to know the F -symbols describing the change of basis as given in Fig. 7, for the case of $SU(2)$ spin-1/2's, i.e. $\alpha_i = \alpha_{i+1} = 1/2$. The F -symbols are closely related to the Wigner $6j$ -symbols [see, for instance Ref. 53 or the $SU(2)_k$ F -symbols with $q = 1$ (i.e. $k = \infty$) in Appendix A]. The F -symbols of interest here are given by

$$\left[F_{x_{i+1}}^{x_{i-1}, \frac{1}{2}, \frac{1}{2}} \right]_{x_i, \tilde{x}_i} = (-1)^{x_{i-1} + x_{i+1} + 1} \times \sqrt{(2x_i + 1)(2\tilde{x}_i + 1)} \begin{Bmatrix} x_{i-1} & 1/2 & x_i \\ 1/2 & x_{i+1} & \tilde{x}_i \end{Bmatrix} \quad (9)$$

where $\tilde{x}_i = 0, 1$ is the total spin of the two spin- $\frac{1}{2}$'s, and $\begin{Bmatrix} j_1 & j_2 & j_{12} \\ j_3 & j & j_{23} \end{Bmatrix}$ denote the $6j$ -symbols.

In particular, if $x_{i+1} = x_{i-1} \pm 1$, then the value of x_i and \tilde{x}_i are fixed to be $x_i = x_{i-1} \pm \frac{1}{2}$ and $\tilde{x}_i = 1$, and the resulting F -symbol is just a number, namely

$$\left[F_{x_{i-1} \pm 1}^{x_{i-1}, \frac{1}{2}, \frac{1}{2}} \right]_{x_{i-1} \pm \frac{1}{2}, 1} = 1. \quad (10)$$

In the case that $x_{i-1} = x_{i+1} = 0$, we must have $x_i = 1/2$ and $\tilde{x}_i = 0$. The associated F -symbol is again 1,

$$\left[F_0^{0, \frac{1}{2}, \frac{1}{2}} \right]_{\frac{1}{2}, 0} = 1. \quad (11)$$

The only case for which the F -symbol has rank two is when $x_{i-1} = x_{i+1} = s \geq \frac{1}{2}$, giving $x_i = s \pm \frac{1}{2}$ and $\tilde{x}_i = 0, 1$. The F -symbol takes the form

$$F_s^{s, \frac{1}{2}, \frac{1}{2}} = \frac{1}{\sqrt{2s+1}} \begin{bmatrix} -\sqrt{s} & \sqrt{1+s} \\ \sqrt{1+s} & \sqrt{s} \end{bmatrix} \quad (12)$$

where the first column corresponds to $\tilde{x} = 0$, and the second one $\tilde{x} = 1$.

With the knowledge of the F -symbols, we can construct the Hamiltonian [see Fig. 8(a)], which symbolically takes the form

$$\begin{aligned} \left[h_{x_{i+1}}^{x_{i-1}, \frac{1}{2}, \frac{1}{2}} \right]_{x_i, x'_i} &= V \delta_{x_i, x'_i} \\ &- J \left[F_{x_{i+1}}^{x_{i-1}, \frac{1}{2}, \frac{1}{2}} \right]_{x_i, 0} \left[(F_{x_{i+1}}^{x_{i-1}, \frac{1}{2}, \frac{1}{2}})^{-1} \right]_{0, x'_i} \end{aligned} \quad (13)$$

where we included the coulomb interaction V , because the electrons occupy neighboring sites, and we favor the spin-0 channel (implicitly it is only non-zero if the diagram is allowed by the fusion rules). Explicitly, we find that $h_{x_{i+1}}^{x_{i-1}, 1/2, 1/2} = V$ in the case that $x_{i+1} \neq x_{i-1}$. For $x_{i-1} = x_{i+1} = 0$, we have $h_0^{0, 1/2, 1/2} = V - J$, and for $s > 0$, we have

$$h_s^{s, 1/2, 1/2} = \begin{bmatrix} V - \frac{Js}{2s+1} & \frac{J\sqrt{s(1+s)}}{2s+1} \\ \frac{J\sqrt{s(1+s)}}{2s+1} & V - \frac{J(s+1)}{2s+1} \end{bmatrix}. \quad (14)$$

The Hamiltonian in the case of Ising and Fibonacci anyons [see Figs. 8(b,c)] is obtained in the same way as we did above for spin-1/2 electrons. The most important necessary ingredient are the F -symbols, which can be found in Appendix A.

For Ising anyons, the non-zero matrix elements are limited to

$$\left[h_I^{I, \sigma, \sigma} \right]_{\sigma, \sigma} = \left[h_\psi^{\psi, \sigma, \sigma} \right]_{\sigma, \sigma} = V - J \quad (15)$$

$$\left[h_\psi^{I, \sigma, \sigma} \right]_{\sigma, \sigma} = \left[h_I^{\psi, \sigma, \sigma} \right]_{\sigma, \sigma} = V \quad (16)$$

and

$$h_\sigma^{\sigma, \sigma, \sigma} = \begin{bmatrix} V - J/2 & -J/2 \\ -J/2 & V - J/2 \end{bmatrix}, \quad (17)$$

where the basis used to write the matrix is $\{I, \psi\}$.

The non-zero matrix elements of the Fibonacci chain are given by

$$\left[h_I^{I, \tau, \tau} \right]_{\tau, \tau} = V - J \quad (18)$$

$$\left[h_\tau^{I, \tau, \tau} \right]_{\tau, \tau} = \left[h_I^{\tau, \tau, \tau} \right]_{\tau, \tau} = V \quad (19)$$

and

$$h_\tau^{\tau, \tau, \tau} = \begin{bmatrix} V - J/\phi^2 & -J/\phi^{3/2} \\ -J/\phi^{3/2} & V - J/\phi \end{bmatrix}, \quad (20)$$

where ϕ is the golden ratio and the matrix is written in the basis $\{I, \tau\}$.

E. Anyon ‘‘hopping’’

Finally, we have to consider the possibility for quasiparticles (including the vacuum I) to move on the lattice and gain kinetic energy. The (effective) physical hopping processes are shown in Fig. 9. In such a move, the entire quasiparticle, including the electric charge and spin/topological charge, is transported from one lattice site to a vacant site that is adjacent to it. (Generally, ‘‘hopping’’ may involve transfer of a quasiparticle to an occupied site, but we do not consider such processes in our models.) Note that the magnitude of the hopping t is not affected by the truncation of the Hilbert space to the reduced space of the low-energy quasiparticles. Note also that the sign of t is irrelevant, so one can assume $t > 0$ for simplicity.

When $|J|$ is large in comparison to t and V , the system phase-separates i.e. the anyons tend to form large clusters of higher density $\rho \simeq 1$. In contrast, for larger kinetic energy (i.e. t) and/or repulsion between the anyons, the system remains homogeneous. This is the regime of interest here and, for $\rho = 2/3$ and $\rho = 1/2$, we have found that it is realized for $t = |J|$, even when $V = 0$, or larger $t/|J|$ values. Note that for convenience we assume $V = 0$ throughout and we have explored the models for values of J ranging from $-t$ to t .

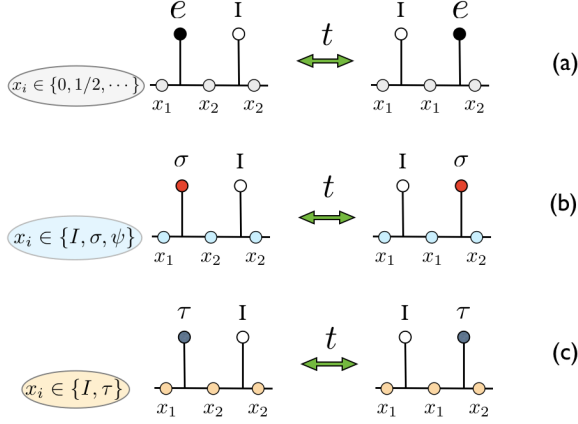


FIG. 9: Tunneling process (or “hopping”) of (a) an electron, (b) an Ising anyon, and (c) a Fibonacci anyon.

IV. CHARGE DEGREES OF FREEDOM FOR $J = 0$

This section is a “warm-up” for the real itinerant anyon models, starting with the simple example of identical bosons, and describes how making them distinguishable introduces a twist in the periodic boundary conditions. It therefore explains the $J = 0$ part of the spectra, without the non-Abelian complications.

A. Hard-core bosons

We start with a periodic chain of size L filled with N bosons. We consider the case where two bosons cannot occupy the same site due e.g. to an infinite on-site repulsion (hard-core constraint). Such a system of hard-core bosons (HCBs) can be mapped via a Holstein-Primakoff and Jordan-Wigner transformation onto a gas of spinless fermions. In 1D, the effect on the spectrum due to the difference in statistics can simply be accounted for by adding to the fermions an extra phase shift of π through the ring (when the particle number $N = \rho L$ is even). Therefore, the HCB many-body spectrum can be obtained by filling up N states of a (fermionic) cosine band,

$$E_{\text{HCB}}(p) = -2t \sum_{j(p)} \cos \left[\frac{2\pi}{L} \left(j + \frac{1}{2} \right) \right], \quad (21)$$

where $\{j(p)\}$ is a set (labelled by p) of an even number N of different integers and the momenta are all shifted by π/L . The spectrum (for $t = 1$) is displayed in Fig. 10(a). As expected, the HCB spectra exhibit linear quasiparticle dispersions centered at momenta $K = 0$ and $K = K_c \equiv 2\pi\rho$ [or $2\pi(1 - \rho)$ for $\rho > 1/2$].

For later use in the case of anyons, it is of interest to introduce an external magnetic flux ϕ_{ext} or equivalently

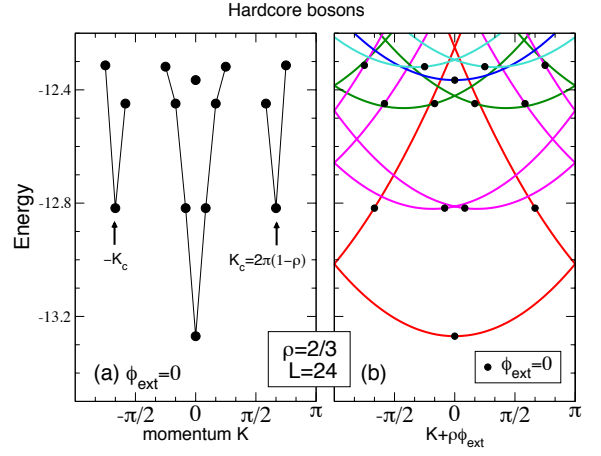


FIG. 10: Spectra of 16 (hardcore) bosons moving on a 24-site chain with PBC. (a) Spectrum for zero magnetic flux through the ring. The linear dispersions vs momentum K are shown at $K = 0$ and $K = \pm K_c$. (b) Spectrum vs. external (continuous) magnetic flux ϕ_{ext} (multiplied by the density ρ). Each discrete level (black dots) leads to a (parabolic) branch of excitations.

an Abelian U(1) flux through the ring. The new spectrum $E_{\text{HCB}}(p, \phi_{\text{ext}})$ depends now on both discrete and continuous variables p and ϕ_{ext} ,

$$E_{\text{HCB}}(p, \phi_{\text{ext}}) = -2t \sum_{j(p)} \cos \left[\frac{2\pi}{L} \left(j + \frac{1}{2} \right) + \frac{\phi_{\text{ext}}}{L} \right], \quad (22)$$

plotted in Fig. 10(b) (for $t = 1$). The state labelled by (p, ϕ_{ext}) now carries an arbitrary (continuous) total momentum $\tilde{K} = K_p + \rho\phi_{\text{ext}}$ with $K_p = \frac{2\pi}{L} \sum_{j(p)} (j + \frac{1}{2})$.

B. Fermions and anyons

We now make the (quasi)particles *distinguishable*, i.e. we introduce some internal degrees of freedom which can be e.g. the spin-1/2 components of the electrons or the anyonic degrees of freedom of the Ising σ or Fibonacci τ anyons. The resulting model is the same as considering the above t - J models in the limit where $J = 0$ (t can be set to 1). This limit, where the energy scale of the anyonic degrees of freedom are set to zero, is of great interest since it provides insight on the nature of the charge excitations.

In that limit, the mobile anyons are expected to still behave as HCB. However, the extra internal degrees of freedom (with zero energy scale) should provide extra features on top of the HCB spectrum. Because of the anyonic (or spin) degrees of freedom linked to them the charged bosons are no longer indistinguishable particles and, on a torus or a ring, hopping of a particle across the “boundary” cyclically translates the labels of the fusion tree. To recover the same labeling, in general, all N particles must be translated over the boundary. Thus, one distinguishable particle hopping over the boundary

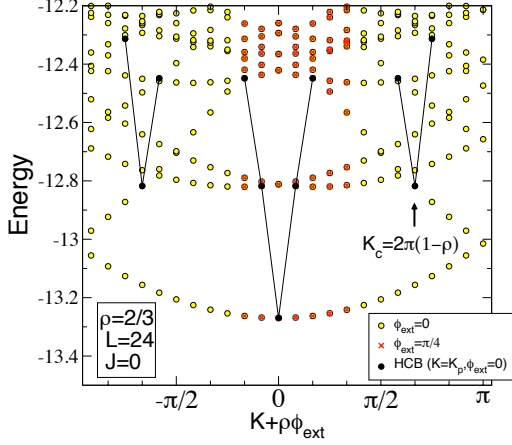


FIG. 11: Low-energy spectrum of a 24-site t - J chain at $J = 0$ and density $\rho = 2/3$, obtained numerically using Ising anyons. Yellow circles correspond to the spectrum at $\phi_{\text{ext}} = 0$ as a function of momentum K . The “parent” charge excitations (HCB at $\phi_{\text{ext}} = 0$) are shown by full (black) circles. Adding an external flux ϕ_{ext} through the ring is equivalent to shift K by $\rho\phi_{\text{ext}}$: the (red) \times symbols correspond to the spectrum at $\phi_{\text{ext}} = \pi/4$ restricting $K \in [-\pi/3, \pi/6]$ (so that $\tilde{K} \in [-\pi/6, \pi/3]$).

has the same effect as a phase shift $\phi_n = 2\pi \frac{n}{N}$ (with n an integer). Hence the complete $J = 0$ electronic/anyonic spectrum (at zero external flux) is given by the union of all HCB spectra taken at all discrete values of ϕ_n ,

$$E_{\text{charge}}^{p,n} = E_{\text{HCB}}(p, \phi_n). \quad (23)$$

A momentum shift is induced by the $U(1)$ flux, given by $\rho\phi_n$ i.e. $2\pi \frac{n}{L}$, an integer multiple of $\frac{2\pi}{L}$. The states then carry (discrete) total momenta,

$$K_{p,n} = K_p + 2\pi \frac{n}{L}, \quad (24)$$

where K_p are the momenta of the HCB eigenstates at $\phi_{\text{ext}} = 0$. For convenience one can distribute the phase shift equally on the bonds to preserve translational invariance and one gets,

$$E_{\text{charge}}^{p,n} = -2t \sum_{j(p)} \cos \left[\frac{2\pi}{L} \left(j + \frac{1}{2} + \frac{n}{N} \right) \right]. \quad (25)$$

Spectra for Ising and Fibonacci anyons obtained by exact diagonalization (ED) for $J = 0$ are shown in Fig. 11 and Fig. 12(a,b). As expected, Eq. (25) matches exactly the numerical exact diagonalization results. From the above considerations, it is then clear that the eigen-energies lie exactly on top of the parabolas corresponding to the “optical” excitations of the HCB. In other words, each state in the HCB spectrum is extended into a discrete set of levels on a parabola – the same parabola that one gets by adding flux (an Abelian phase), as checked numerically.

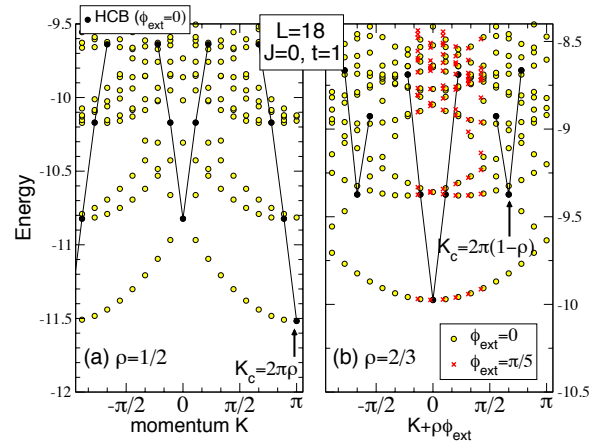


FIG. 12: Low-energy spectra vs. momentum K of a 18-site t - J chain with $J = 0$ at anyon densities (a) $\rho = 1/2$ and (b) $\rho = 2/3$. The notations here are the same as in Fig. 11, but these results are obtained numerically using Fibonacci anyons. The low-energy spectra of the 18-site HCB chain at the same densities (parent excitations) are shown by black dots. Data for an external flux $\phi_{\text{ext}} = \pi/5$ are shown in (b). The minimum of the spectrum occurs at momentum $K = 0$ or $K = \pi$, depending on the parity of the number $N = \rho L$ of quasiparticles.

It is important to notice that the $J = 0$ spectrum does not depend on the internal degrees of freedom and, hence, on the nature of the quasiparticles, i.e. whether they are electrons, Ising anyons, Fibonacci anyons, or distinguishable bosons. However, the respective Hilbert spaces are very different which means that the corresponding eigenfunctions and degeneracies differ completely. In addition, the way the very large degeneracy of each level is lifted by any finite exchange interaction (see Fig. 14 discussed later) depends crucially on the type of particles.

C. External magnetic flux

When the anyons experience an arbitrary *external* flux ϕ_{ext} , the above formula can be generalized to $E_{\text{charge}}^{p,n}(\phi_{\text{ext}}) = E_{\text{HCB}}(p, \phi_n + \phi_{\text{ext}})$. It then becomes apparent that the $J = 0$ energy spectrum does not depend on the momentum $K_{p,n}$ and external flux ϕ_{ext} separately but rather only on the “pseudo-momentum” combination $\tilde{K} = K_{p,n} + \rho\phi_{\text{ext}}$. Hence, one can define a spectrum depending on both discrete and continuous variables,

$$E_{\text{charge}}(p, \Phi) = E_{\text{HCB}}(p, \Phi). \quad (26)$$

The curvature of the ground-state energy $\partial^2 E_{\text{charge}}(0, \Phi) / \partial \Phi^2$ is directly proportional to the optical (Drude) weight quantifying the potential of this system to conduct.

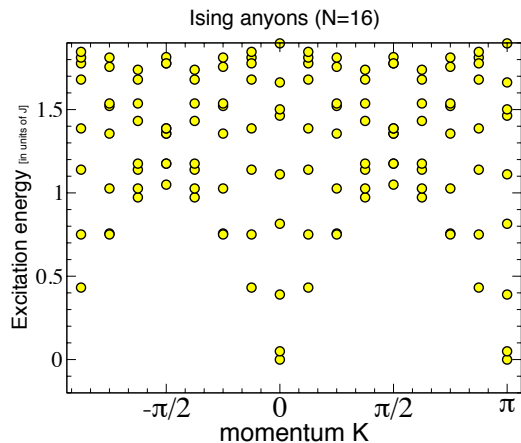


FIG. 13: Energy spectrum of a dense Ising-anyon chain ($\rho = 1$) of length $L_a = 16$. The ground state energy has been subtracted.

V. DENSE ANYON MODELS

To complete the warmup to describe the full anyonic t - J model, we briefly discuss the dense anyon models at $\rho = 1$. These models have precisely one anyon per site, which are, hence, immobile due to the hard-core constraint. Every anyon interacts with its two neighbors, and only the sign of the interaction strength J is relevant. These models, introduced in Ref. 54, are the anyonic versions of the Heisenberg spin chains. We will only consider the spin-1/2 versions in this paper.

In the case where only a nearest-neighbor two-body interaction is present, the spin-1/2 anyonic chains are all critical, and their energy spectra are described by well known conformal field theories. Starting with the Ising anyons, we note that, due to the fusion rules, the degrees of freedom on the fusion chain are forced to form a pattern of alternating frozen σ bonds and bonds fluctuating between I and ψ . For these later bond variables, the interactions of Fig. 7(c) are exactly those of a *critical Ising model in transverse field* whose corresponding CFT has central charge $c = 1/2$. This is irrespective of the overall sign of the interaction, although the momenta at which the various states occur differ depending on the sign of J .

In the case of Fibonacci anyons, changing the sign of J does alter the critical behavior of the chain. In the case of anti-ferromagnetic interactions (favoring the trivial fusion channel of two neighboring Fibonacci anyons), the critical behavior is described in terms of the $c = 7/10$ tri-critical Ising model, with low-lying, linearly dispersing modes occurring at momenta $K = 0$ and $K = \pi$. For ferromagnetic interactions, the critical behavior is instead described by the $c = 4/5$ 3-state Potts model, which exhibits low-lying modes at $K = 0, 2\pi/3, 4\pi/3$.

The behavior described above can be obtained by mapping the models onto exactly solvable two-dimensional

height models, introduced by Andrews, Baxter and Forrester.⁵⁵ The result for spin-1/2 anyons associated with $SU(2)_k$ is that in case of anti-ferromagnetic interactions, the critical behavior of the chain is given in terms of the k -critical Ising model, while ferromagnetic interactions give rise to the critical behavior of the \mathbb{Z}_k -parafermions.

We would like to stress that, although one can analytically obtain the critical behavior of the dense anyonic chains, it is not possible to obtain the energy spectra in full detail for finite size systems for $k \geq 3$. To obtain these, one must employ numerical techniques, such as exact diagonalization (see e.g. Fig. 13, for the $k = 2$ Ising case, which can also be obtained exactly). In describing the full spectra of the anyonic t - J models, we will make use of the spectra of the dense anyonic models described here, as obtained from exact diagonalization.

We will denote the length of the dense anyon chains by L_a . The energies of the dense anyon chains are denoted by $E_{\text{anyon}}(m)$, where the integer m labels the eigenstates, which have momenta k_m that are integer multiples of $2\pi/L_a$. Next, considering chains of length L and at anyon densities $\rho < 1$, we shall define the corresponding “squeezed chains” of dense anyons of length $L_a = \rho L = N$, in which the vacancies (or trivial quasiparticles) have been removed.

VI. MANY-BODY SPECTRA OF THE ANYONIC t - J MODELS

Having described the spectra of the HCB system, in the presence of external flux, as well as the spectra of dense anyon models, we are now ready to describe the spectra of the full, itinerant anyon models. We will label the various energies as $E_{p,m}$, where the labels p and m refer to the (renormalized) HCB spectrum and the dense anyon chain, respectively. We will also explain the subtle coupling of the momenta.

A. Separation of charge and anyonic degrees of freedom

We now consider to the full $J > 0$ spectra of the itinerant models. We solve the effective anyonic models on small periodic rings using exact diagonalization. For Ising anyons, a 24-site chain is studied at density $\rho = 2/3$ ($N = 16$ quasiparticles). For Fibonacci anyons (which have a larger Hilbert space) we consider a 18-site chain at density $\rho = 1/2$ ($N = 9$ quasiparticles) and $\rho = 2/3$ ($N = 12$ quasiparticles). We choose $|J| \leq t$ for which the system remains uniform and does not phase separate (which occurs for larger J). Note that the sign of J is irrelevant for the energy levels in the case of Ising anyons, though the momenta at which the various states occur differs depending on the sign of J .

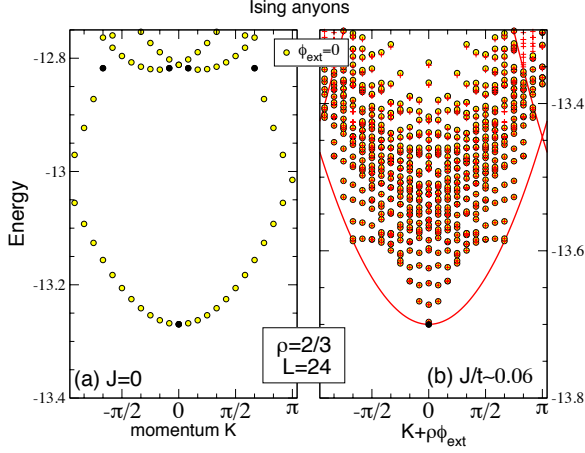


FIG. 14: A zoom-in on the low-energy spectra vs. K of a 24-site Ising anyon t - J chains at density $\rho = 2/3$ for (a) $J = 0$ and (b) a small value of $J/t = \tan(\pi/50) \simeq 0.06$. The Lanczos algorithm with 800 iterations is used so that, in the shown energy window, most of the eigen-energies have converged to within a relative error of 10^{-16} (a few not-fully converged levels are not shown). The (red) + symbols correspond to the sum of the (computed) lowest charge branch (continuous red line) with *all* the expected anyonic excitations. (See text for more details.)

The low-energy spectra ($|J| = t = 1/\sqrt{2}$) of the itinerant Ising and Fibonacci anyonic chains are shown in Figs. 15(b) and Fig. 16(a,b), respectively. These seem very different from the $J = 0$ limit studied above (and shown again in Fig. 15(a) for comparison). To understand such spectra, let us first consider a zoom-in on the low-energy region and compare the spectra at $J = 0$ and at a small value of J , as shown in Figs. 14(a,b). This reveals that the *highly degenerate* $J = 0$ charge excitation parabola is being split by the magnetic interaction into a complex spectrum with a spread in energy proportional to JL . When $J \sim t/L^2$, the spectra originating from each parabola start to overlap as expected in Figs. 15(b) and 16(a,b). Despite the apparent complexity of the $J \neq 0$ spectrum, we shall be able to express all excitations as the sum of an anyonic excitation and a charge excitation, extending the concept of spin-charge separation familiar for 1D correlated electrons to the case of a 1D anyonic interacting system. To complete this task, we first establish from simple considerations the “recipes” to construct separately the expected charge and anyonic spectra. In a second step, we show how the numerical spectra of the t - J anyonic chains can be seen as a subtle combination of the above two spectra.

The Bethe ansatz results^{56–58} for the $J \rightarrow 0$ *electronic* t - J chain suggest that the anyonic contributions, $E_{\text{anyon}}(m)$, to the excitation spectrum of the itinerant anyon chain are those of the *squeezed* periodic chain of localized anyons produced by removing all vacant sites, which has the resulting length $L_a = N = \rho L$. Here,

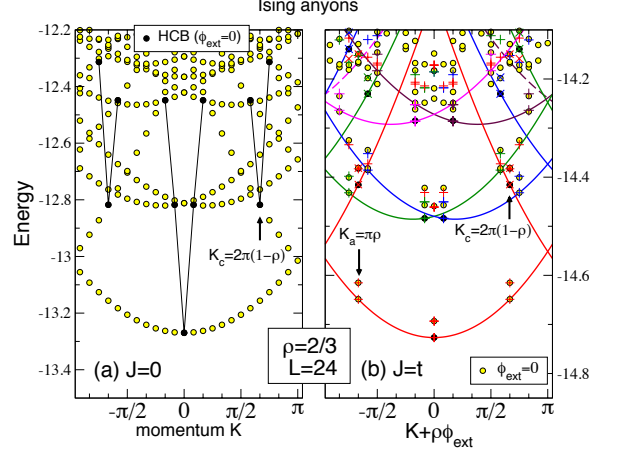


FIG. 15: Low-energy spectra vs. K of a 24-site Ising t - J chain at density $\rho = 2/3$ for (a) $J = 0$ and (b) $J = t = 1/\sqrt{2}$. The data at $\phi_{\text{ext}} = 0$ are shown by yellow circles. The parent charge excitations are shown by black dots ($\phi_{\text{ext}} = 0$) and, as a function of pseudo-momentum $\tilde{K} = K + \phi_{\text{ext}}\rho$ (varying ϕ_{ext}), by continuous lines of different colors. The + and \times symbols added for comparison correspond to the sum of the charge and expected anyonic excitation spectra. (See text for more details.) The colors of these symbols are the same as their *parent* charge excitation parabolas.

the integer m labels the eigenstates of momenta k_m , which are multiples of $2\pi/L_a$. Such a spectrum can be computed separately by exact diagonalization and agrees very well with the CFT predictions, even on small chains ($L_a = 12, 16$). In particular, it shows a (linear) zero energy mode at zero momentum and at a characteristic momentum k_a , where $k_a = \pi$ for Ising and $J > 0$ Fibonacci chains and $k_a = 2\pi/3$ for $J < 0$ Fibonacci chains. The coupling constant providing the scale of the anyon spectrum is expected to be weakly renormalized from J to γJ in the doped system, where γ is a factor of order 1 that is to be adjusted as we described below.

To construct the expected charge excitation spectrum at finite J , we use our understanding of the charge excitations in the $J = 0$ limit. Starting from $J = 0$ and turning on J gradually, one can *a priori* adiabatically follow the original ($\Phi = 0$) HCB excitations evolving in, what we call, the *parent* charge excitations at $J \neq 0$ (labelled by the same integers p and at the same momenta K_p). As for $J = 0$, changing the momentum K of a charge excitation amounts to introducing a total phase shift (or flux) $\Phi = K/\rho$. Hence, by introducing “twisted boundary conditions” one can *compute* numerically the (almost parabolic) branch of excitations $\tilde{E}_{\text{charge}}(p, \Phi)$ associated to each parent excitation (labelled by p). Note that each branch is “renormalized” by J so that, strictly speaking, the charge spectrum is no longer associated to *non-interacting* spinless fermions (i.e. to HCBs) and, hence, is no longer given by a simple analytic expression as in Eq. (26). How-

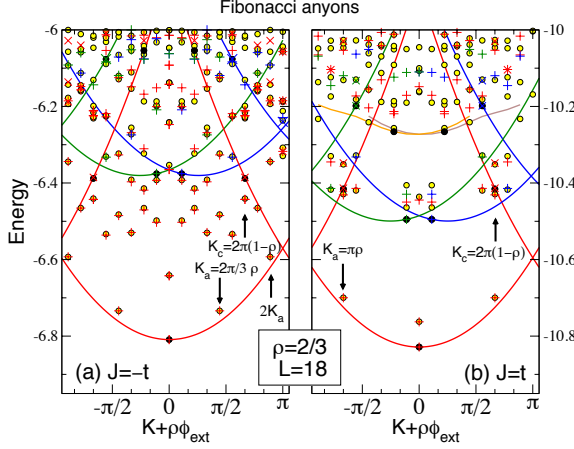


FIG. 16: Low-energy spectra vs. K of a 18-site Fibonacci t - J chain at density $\rho = 2/3$ and $|J| = t = 1/\sqrt{2}$ for both (a) $J < 0$ and (b) $J > 0$. The data at $\phi_{\text{ext}} = 0$ are shown by yellow circles. The parent charge excitations are shown by black dots ($\phi_{\text{ext}} = 0$) and, as a function of pseudo-momentum $\tilde{K} = K + \rho\phi_{\text{ext}}$ (varying ϕ_{ext}), by continuous lines of different colors. The + and \times symbols added for comparison correspond to the sum of the charge and (expected) anyonic excitation spectra (see text). The color of these symbols is the same as their parent charge excitation parabola.

ever, if different parent states lie on the same branch, they are still exactly spaced apart by integer multiples of $\Delta\Phi = 2\pi$ i.e. $\tilde{E}_{\text{charge}}(p, \Phi) = \tilde{E}_{\text{charge}}(p', \Phi + 2k\pi)$ where $K_{p'} - K_p = 2k\rho\pi$, for some integer k .

We now explain how to construct the full excitation spectrum by simply considering that (i) the charge degrees of freedom are subject to a phase shift in the boundary conditions and (ii) the anyonic degrees of freedom are the ones of the *squeezed* periodic anyonic chain. According to the above arguments, the energy excitation spectrum should be given by adding the two contributions,

$$E_{p,m} = \tilde{E}_{\text{charge}}(p, k_m) + E_{\text{anyon}}(m). \quad (27)$$

A natural prescription is to simply add the momenta: $K = K_p + \rho k_m$. In other words, we assume that the phase shift experienced by the charged “holons” coincides with the total momentum $k_m = \frac{2\pi n_m}{L_a}$ (where n_m is an integer) of the anyonic eigenstates defined on the squeezed (undoped) chain. These rules for adding charge and anyonic momenta are therefore assumed to be similar to the $J \rightarrow 0$ Bethe ansatz.

We now wish to verify that proper assignments of the true energy levels according to the form given by Eq. (27) can indeed be made accurately. First, we consider adding a very small exchange coupling J which lifts the very large degeneracy of the low-energy parabola of the HCBs (see Fig. 14). For finite J the first charge branch (with $E_{\text{anyon}} = 0$) originating from the zero-momentum ground-state of the model (which we assign $p = 0$) can be computed by adding an Abelian flux to

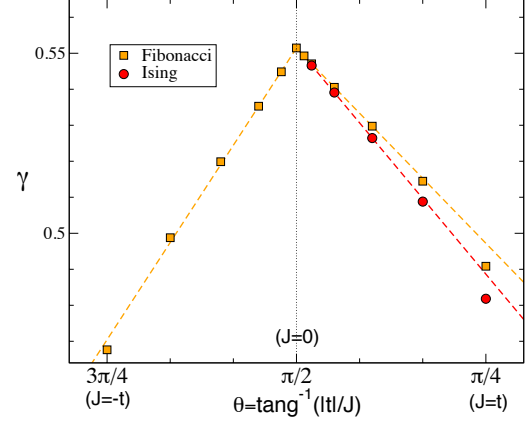


FIG. 17: Renormalization parameter γ of the energy scale of the anyonic degrees of freedom for Ising and Fibonacci at $\rho = 2/3$, computed on $L = 24$ and $L = 18$ chains, respectively.

the system. It is then possible to construct the expected set of combined charge plus anyon excitations $E_{0,m}$ by adjusting the renormalization factor γ to get the best fit to the exact low-energy levels. Although there is only one free parameter, it is remarkable that *all* anyon excitations above the lowest charge parabola can be assigned very accurately as seen in Fig. 14(b).

When $|J| \sim t$, charge and anyonic excitations have the same energy scale and one must proceed step by step, sequentially constructing the sets of levels corresponding to increasing charge index p . The two “secondary” parent charge excitations corresponding to exact eigenstates of the system with momenta $K_p = \pm K_c$ ($p = 1, 2$) lie on the *same* $p = 0$ branch, as seen on Figs. 15(b) and 16(a,b). These states lead to the secondary level of combined excitations $E_{1,m}$ and $E_{2,m}$, with no further adjustable parameter. Recall that $K_c = 2\pi\rho$ if $\rho \leq 1/2$ and $K_c = 2\pi(1 - \rho)$ for $\rho > 1/2$. Next, in a second step, we identify the lowest *not yet assigned* excitations at momenta $K_p = \pm 2\pi/L$ as the subsequent pure charge excitations (and assign them the labels $p = 3, 4$). Following these levels adiabatically under the addition of a flux enables us to construct the corresponding charge branches and locate the secondary pure charge excitation at momenta $K_p = \pm(2\pi/L + K_c)$ (called $p = 5, 6$). Then, as before, the combined excitations $E_{p,m}$, $p = 3, \dots, 6$, can be constructed. One can repeat this procedure (going up in energy) until the level density and the number of charge branch crossings becomes too large to make precise assignments. In practice, we have identified up to $p = 11$ pure charge excitations and their corresponding low-energy combined anyonic-charge excitations for the Ising chain, as shown in Fig. 15(b). For the Fibonacci chains, we have identified up to $p = 9$ pure charge excitations and their corresponding low-energy combined anyonic-charge excitations, as shown in Fig. 16(a,b).

Our results show that the anyonic energy spectrum

is basically given by the same type of Bethe ansatz as for the electronic t - J model (in the $J/t \rightarrow 0$ limit)^{56,57} and, in particular, (i) the $J = 0$ charge excitation spectrum is *exactly the same*, (ii) the spin excitations also correspond to the squeezed localized chain, and (iii) the rules for adding charge (holon) and spin/anyon momenta are *identical*. In addition, the numerical spectra agree very well with the sum of the spin (provided some renormalization γ of the energy scale, as shown in Fig. 17) and charge spectra (constructed independently) with the above-mentioned rule for momentum conservation. We believe the small deviations can be attributed to finite size effects (which vanish when $J/t \rightarrow 0$). Interestingly, the $J \rightarrow 0$ limit of the renormalization parameter γ , $\gamma(0) \simeq 0.5515$ for $\rho = 2/3$, is independent on the anyon type (as the $J = 0$ charge excitation spectrum). In fact, in this limit, it should only depend on the probability of having two neighboring anyons.

B. Anyonic and charge collective excitations

Due to the above decoupling, the collective anyonic and charge excitations can be deduced easily from the above excitation spectra, by just applying selection rules. Charge excitations occur between different charge branches at constant m with energy transfer

$$\mathcal{E}_{p',p;m} = \tilde{E}_{\text{charge}}(p', k_m) - \tilde{E}_{\text{charge}}(p, k_m), \quad (28)$$

and momentum transfer $K = K_{p'} - K_p$. Anyonic excitations are characterized by $\Delta p = 0$ and are then given by

$$\begin{aligned} \mathcal{E}_{p;m',m} &= E_{\text{anyon}}(m') - E_{\text{anyon}}(m) \\ &+ \tilde{E}_{\text{charge}}(p, k_{m'}) - \tilde{E}_{\text{charge}}(p, k_m), \end{aligned} \quad (29)$$

with momentum transfer $K = \rho(k_{m'} - k_m)$. Note that the last two terms in Eq. (29) give a finite size correction in the energy of order $1/L^2$. In the thermodynamic limit, zero-energy anyonic excitations occur at momentum $K_a = \rho k_a$ (and $2K_a$ if different), where k_a is the characteristic momentum (introduced above) of the zero-energy mode of the pure chain. The location of both charge and anyonic zero-energy modes are indicated in Fig. 15(b) for Ising anyons and in Figs. 16(a,b) for Fibonacci anyons.

C. Form of the eigenstates

We now discuss briefly the structure of the eigenfunctions. Eq. (2.14) of Ref. 56 established that the ground-state of the $J \rightarrow 0$ limit of the electronic t - J chain can be written exactly as a product of a charge HCB wavefunction times a spin wavefunction identical to the ground-state of the 1D $S = 1/2$ Heisenberg model. Our results suggest that a similar product structure might in fact also

hold in the case of *all low-energy eigenstates* of 1D non-Abelian anyons at $J \neq 0$, up to *finite size corrections*. We speculate that the eigenfunctions can be approximately written as,

$$\begin{aligned} \Psi_{p,m}(y_1, \dots, y_N; x_1, \dots, x_N) &\simeq \tilde{\Phi}_{\text{charge}}^p(y_1, \dots, y_N) \\ &\times \chi_{\text{anyon}}^m(x_1, \dots, x_N), \end{aligned} \quad (30)$$

where y_j are the position of the (site) anyons on the L -site chain and x_i are the bond variables associated to them (see Fig. 1). Here, $\tilde{\Phi}_{\text{charge}}^p$ are the eigenstates (labelled by p) of an *interacting* L -site HCB chain in the presence of a twist (i.e. flux) k_m in the boundary conditions and χ_{anyon}^m are the eigenstates (labelled by m) with momentum k_m of the interacting (undoped) anyonic chain of $L_a = \rho L$ sites.

VII. DMRG STUDY OF THE MODEL

We can use DMRG to compute the resulting CFT central charge from the analysis of the von Neumann entanglement entropy (EE) of an open chain (of length L) cut into two subsystems⁵⁹. We focus here on the case of the diluted Fibonacci t - J chain with $\rho = 2/3$ and $J > 0$, for which we expect the anyonic part to be described by a $c = 7/10$ tri-critical Ising CFT. In Fig. 18, we plot the ground state's EE

$$S_A = S_B = -\text{Tr}[\rho_A \log \rho_A] \quad (31)$$

between subsystems A and B , which are two connected segments of the open chain, as a function of the position of the cut along the chain. The calculation is somewhat non-standard (compared to usual spin systems) because the anyonic fusion tree bond variable x_j labeling the j th link, which connects the two subsystems, i.e. the link across which one “cuts” the system in two, is shared by both subsystems of the chain. This shared link variable characterizes the overall topological charge of each subsystem. The reduced density matrices

$$\rho_A = \text{Tr}_B \rho, \quad \rho_B = \text{Tr}_A \rho \quad (32)$$

of subsystems A and B are block diagonal with respect to this variable, i.e.

$$\rho_A = \bigoplus_{x_j} p_{x_j} \rho_{A,x_j}, \quad (33)$$

where $p_{x_j} = \text{Tr}[\Pi_{x_j} \rho]$ is the probability that the state will have topological charge x_j on the j th link, and $\rho_{A,x_j} = \frac{1}{p_{x_j}} \text{Tr}_A[\Pi_{x_j} \rho]$ is the reduced density matrix for subsystem A after projecting the j th link's variable onto the value x_j .

In order to verify that this Fibonacci t - J chain results in a CFT with central charge $c = 1.7$, we fit to the formula⁵⁹⁻⁶⁴

$$S(j) = a + b p_{x_j=\tau} + \frac{c}{6} \log \left[L \sin \left(\frac{\pi j}{L} \right) \right], \quad (34)$$

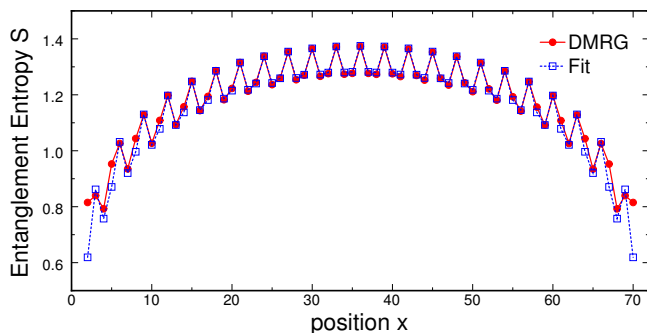


FIG. 18: Entanglement entropy obtained using DMRG for an open chain of length $L = 72$, with $N = 48$ Fibonacci anyons, and $J/t = 0.3$. The EE predicted for a CFT with central charge $c = 1.7$ is plotted and the agreement is seen to be excellent.

where a and b are fitting parameters. The first term is a non-universal constant, which can include universal contributions, such as a boundary entropy. The second term is a phenomenologically motivated correction that is proportional to a local kinetic energy, i.e. $p_{x_j=\tau} = \langle n_{\text{link}}(j) \rangle$ where $n_{\text{link}}(j)$ is the density (occupation) operator of the j th link, and can include a contribution due to the boundary between the two subsystems. The third term is derived from CFT. We find the best fit for the parameter values $a = 0.31185$ and $b = -0.35547$. As seen in Fig. 18, the agreement between the numerical results and the values provided by this expression is excellent.

VIII. CONCLUSION AND OUTLOOK

Motivated by the possible realization of non-Abelian Ising and Fibonacci quasiparticles in quantum Hall states and Majorana heterostructures and the importance of understanding their edge modes, we have investigated what happens if itinerant and interacting (charged) non-Abelian anyons are confined on a 1D chain, subject to a strong charging energy. Following a standard procedure for strongly correlated electronic systems, we have constructed simple low-energy effective models by truncating the Hilbert space to the relevant low-energy particles. Integrating out the high-energy virtual processes yields an “exchange” interaction between anyons, which physically favors a particular fusion channel. The effective model generically takes the form of an anyonic t - J model, containing the exchange interaction (J) and the rate (t) of anyon “hopping” between nearest-neighbor sites. The central result of our work is that anyons fractionalize into their charge and (neutral) anyonic degrees of freedom. This phenomenon closely resembles and generalizes the well-known spin-charge separation in electronic Luttinger liquids. Incidentally, the numerically verification based on the identification of the many-body levels turned out to be more transparent for anyons, due to the absence

of marginally irrelevant operators in the field theory description. The anyon fractionalization justifies *a posteriori* the treatment of the edge theories of these topological phases as a direct product of the charge and neutral non-Abelian modes, even though the electric charge is not localized in current setups.

We note that the 1D electronic t - J model exhibits an exact supersymmetric point^{43,44} at which the full excitation spectrum can be obtained using the Bethe ansatz⁴⁵. It is left for future studies to investigate whether such an integrable point also exists in 1D anyonic t - J models.

Our simple description of interacting itinerant anyons now enables the investigation of realistic setups for manipulating and/or braiding anyons for future quantum computation. It is also easy to extend this study to quasi-1D systems with more than a single conduction channel: anyonic t - J “ladders” could mimic such a case, following the procedure for localized non-Abelian anyons⁶⁵. Whether fractionalization survives in two spatial dimensions is another important issue. Localized anyons were shown to nucleate into a novel *gapped* quantum liquid^{66–69} in two dimensions and a similar scenario might take place for itinerant anyons, with e.g. the anyonic degrees of freedom becoming gapped.

Acknowledgements

DP acknowledges support by the French Research Council (Agence Nationale de la Recherche) under grant No. ANR 2010 BLAN 0406-01. This work was granted access to the HPC resources of CALMIP under the allocation 2012-P1231. DP is also grateful to Nicolas Renon at CALMIP (Toulouse, France) and to SGI (France) for support in the use of the Altix SGI supercomputer. AF acknowledges support by the NSF, Grant No. DMR-0955707. PB and MT thank the Aspen Center for Physics for hospitality and support under the NSF grant #PHY – 1066293.

Appendix A: Examples of Anyon Models

In this Appendix, we give detailed descriptions of the Ising, Fibonacci, and $SU(2)_k$ anyons models, and explain where they occur in non-Abelian quantum Hall states.

1. Ising anyons

The Ising anyon model is derived from the CFT that describes the Ising model at criticality⁷⁰. It is related to $SU(2)_2$ as its CFT can be obtained using the coset construction $SU(2)_2/U(1)_4$. It has topological charges $\mathcal{C} = \{I, \sigma, \psi\}$ (which respectively correspond to vacuum, spin, and Majorana fermions in the CFT, and are sometimes denoted 0, $\frac{1}{2}$, and 1, because of the relation with $SU(2)_2$). The anyon model is described by (listing only

the non-trivial F -symbols and R -symbols, i.e. those not listed are equal to one if their vertices are permitted by fusion, and equal to zero if they are not permitted):

| |
|---|
| $\mathcal{C} = \{I, \sigma, \psi\}, \quad I \times a = a, \quad \sigma \times \sigma = I + \psi,$ $\sigma \times \psi = \sigma, \quad \psi \times \psi = I$ |
| $[F_{\sigma}^{\sigma\sigma\sigma}]_{ef} = \begin{bmatrix} \frac{1}{\sqrt{2}} & \frac{1}{\sqrt{2}} \\ \frac{1}{\sqrt{2}} & -\frac{1}{\sqrt{2}} \end{bmatrix}_{ef}$ $[F_{\psi}^{\sigma\psi\sigma}]_{\sigma\sigma} = [F_{\sigma}^{\psi\sigma\psi}]_{\sigma\sigma} = -1$ |
| $R_I^{\sigma\sigma} = e^{-i\frac{\pi}{8}}, \quad R_{\psi}^{\sigma\sigma} = e^{i\frac{3\pi}{8}},$ $R_{\sigma}^{\sigma\psi} = R_{\sigma}^{\psi\sigma} = e^{-i\frac{\pi}{2}}, \quad R_I^{\psi\psi} = -1$ |
| $d_I = d_{\psi} = 1, \quad d_{\sigma} = \sqrt{2}, \quad \mathcal{D} = 2$ |
| $\theta_I = 1, \quad \theta_{\sigma} = e^{i\frac{\pi}{8}}, \quad \theta_{\psi} = -1$ |

where $e, f \in \{I, \psi\}$.

2. Fibonacci anyons

The Fibonacci anyon model (also known as $\text{SO}(3)_3$, since it may be obtained from the $\text{SU}(2)_3$ anyon model by restricting to integer spins $j = 0, 1$, though $\text{SO}(3)_k$ is only allowed for $k = 0 \bmod 4$; as a Chern-Simons or WZW theory, it may, more properly, be equated with $(\text{G}_2)_1$) is known to be universal for TQC⁷¹. It has two

topological charges $\mathcal{C} = \{I, \tau\}$ (sometimes denoted 0 and 1, respectively, because of the relation with $\text{SU}(2)_3$) and is described by (listing only the non-trivial F -symbols and R -symbols):

| |
|--|
| $\mathcal{C} = \{I, \tau\}, \quad I \times I = I, \quad I \times \tau = \tau, \quad \tau \times \tau = I + \tau$ |
| $[F_{\tau}^{\tau\tau\tau}]_{ef} = \begin{bmatrix} \phi^{-1} & \phi^{-1/2} \\ \phi^{-1/2} & -\phi^{-1} \end{bmatrix}_{ef}$ |
| $R_I^{\tau\tau} = e^{-i4\pi/5}, \quad R_{\tau}^{\tau\tau} = e^{i3\pi/5}$ |
| $d_I = 1, \quad d_{\tau} = \phi, \quad \mathcal{D} = \sqrt{\phi+2} \mid \theta_I = 1, \quad \theta_{\tau} = e^{i\frac{4\pi}{5}}$ |

where $\phi = \frac{1+\sqrt{5}}{2}$ is the Golden ratio.

3. $\text{SU}(2)_k$

The $\text{SU}(2)_k$ anyon models (for k an integer) are “ q -deformed” versions of the usual $\text{SU}(2)$ for $q = e^{i\frac{2\pi}{k+2}}$, which, roughly speaking, means integers n are replaced by $[n]_q \equiv \frac{q^{n/2} - q^{-n/2}}{q^{1/2} - q^{-1/2}}$. These describe $\text{SU}(2)_k$ Chern-Simons theories⁷² and WZW CFTs^{73,74}, and give rise to the Jones polynomials of knot theory⁷⁵. Their braiding statistics are known to be universal for TQC⁷⁶ all k , except $k = 1, 2$, and 4. They are described by:

| |
|---|
| $\mathcal{C} = \{0, \frac{1}{2}, \dots, \frac{k}{2}\}, \quad j_1 \times j_2 = \sum_{j= j_1-j_2 }^{\min\{j_1+j_2, k-j_1-j_2\}} j$ |
| $[F_j^{j_1, j_2, j_3}]_{j_{12}, j_{23}} = (-1)^{j_1+j_2+j_3+j} \sqrt{[2j_{12}+1]_q [2j_{23}+1]_q} \left\{ \begin{matrix} j_1 & j_2 & j_{12} \\ j_3 & j & j_{23} \end{matrix} \right\}_q,$ $\left\{ \begin{matrix} j_1 & j_2 & j_{12} \\ j_3 & j & j_{23} \end{matrix} \right\}_q = \Delta(j_1, j_2, j_{12}) \Delta(j_{12}, j_3, j) \Delta(j_2, j_3, j_{23}) \Delta(j_1, j_{23}, j)$ $\times \sum_z \left\{ \frac{(-1)^z [z+1]_q!}{[z-j_1-j_2-j_{12}]_q! [z-j_{12}-j_3-j]_q! [z-j_2-j_3-j_{23}]_q! [z-j_1-j_{23}-j]_q!} \right.$ $\left. \times \frac{1}{[j_1+j_2+j_3+j-z]_q! [j_1+j_{12}+j_3+j_{23}-z]_q! [j_2+j_{12}+j+j_{23}-z]_q!} \right\},$ $\Delta(j_1, j_2, j_3) = \sqrt{\frac{[-j_1+j_2+j_3]_q! [j_1-j_2+j_3]_q! [j_1+j_2-j_3]_q!}{[j_1+j_2+j_3+1]_q!}}, \quad [n]_q! \equiv \prod_{m=1}^n [m]_q$ |
| $R_j^{j_1, j_2} = (-1)^{j-j_1-j_2} q^{\frac{1}{2}(j(j+1)-j_1(j_1+1)-j_2(j_2+1))}$ |
| $d_j = [2j+1]_q = \frac{\sin(\frac{(2j+1)\pi}{k+2})}{\sin(\frac{\pi}{k+2})}, \quad \mathcal{D} = \frac{\sqrt{\frac{k+2}{2}}}{\sin(\frac{\pi}{k+2})} \mid \theta_j = e^{i2\pi \frac{j(j+1)}{k+2}}$ |

where $\left\{ \begin{matrix} j_1 & j_2 & j_{12} \\ j_3 & j & j_{23} \end{matrix} \right\}_q$ is a “ q -deformed” version of the usual $\text{SU}(2)$ 6j-symbols (which correspond to $q = 1$), and have been calculated in Ref. 77 (see also Ref. 78, for an introduction on how to calculate the F -symbols and an implementation in Mathematica). The sum in the definition of the q -deformed 6j-symbol is over all integers in the range

$$\max\{j_1+j_2+j_{12}; j_{12}+j_3+j; j_2+j_3+j_{23}; j_1+j_{23}+j\} \leq z \leq \min\{j_1+j_2+j_3+j; j_1+j_{12}+j_3+j_{23}; j_2+j_{12}+j+j_{23}\}.$$

4. Moore-Read, anti-Pfaffian, and Bonderson-Slingerland Hierarchy States

The $\nu = 1/m$ MR states⁵ are described by a spectrum restriction of the product of the Ising CFT with an Abelian $U(1)$. Specifically, the anyon model is

$$\text{MR} = \text{Ising} \times U(1)_m|_{\mathcal{C}} \quad (\text{A1})$$

where the restriction to the anyonic charge spectrum \mathcal{C} is such that I and ψ Ising charges are paired with integer $U(1)$ fluxes, while σ Ising charges are paired with half-integer $U(1)$ fluxes. The fundamental quasihole of the MR state has electric charge $e/2m$ (where the particle carries charge $-e$) and carries Ising topological charge σ . The $\nu = 1/2$ MR state is a leading candidate for the experimentally observed $\nu = 5/2$ and $7/2$ quantum Hall plateaus.

Taking the particle-hole conjugate of the MR state yields the aPf state^{7,8}, which is another leading candidate for the $\nu = 5/2$ and $7/2$ quantum Hall plateaus. The anyon model for the aPf state is simply obtained by taking the complex conjugate of the MR state's anyon model.

BS hierarchical states⁹ may be obtained from the MR and aPf states by applying a hierarchical (or, equivalently, a composite fermion) construction to the $U(1)$ sector. The states built on MR may be written as

$$\text{BS}_K = \text{Ising} \times U(1)_K|_{\mathcal{C}} \quad (\text{A2})$$

where the K -matrix is determined by the details of the hierarchical construction over MR, and the spectrum restriction is similar to before. This produces Ising-type candidate states for all other observed second Landau level FQH filling fractions (including those observed at $\nu = 7/3, 12/5, 8/3$, and $14/5$). The quasiparticle excitation spectra of the BS states include excitations that carry the σ Ising topological charge, but these are generally not the unique quasiparticle carrying the minimal electric charge.

5. $k = 3$ Read-Rezayi and NASS

The particle-hole conjugate of the $k = 3, M = 1$ RR state⁶ is a candidate for $\nu = 12/5$, which is constructed from the \mathbb{Z}_3 -Parafermion (Pf_3) CFT and an Abelian $U(1)$. The braiding statistics of this state is described by the direct product of anyon models

$$\overline{\text{RR}}_{k=3,M=1} = \overline{\text{Pf}_3 \times U(1)} = \overline{\text{Fib}} \times \mathbb{Z}_{10}^{(3)}, \quad (\text{A3})$$

where the overline indicates complex conjugation and $\mathbb{Z}_{10}^{(3)}$ is an Abelian anyon model (using the notation of Ref. 79,80). The fundamental quasiholes of this state have electric charge $e/5$ and Fibonacci topological charge τ .

The $k = 2, M = 1$ NASS state²⁰, based on $SU(3)_k$ -parafermions, is a candidate for $\nu = 4/7$. Its braiding statistics is described by

$$\text{NASS}_{k=2,M=1} = \overline{\text{Fib}} \times D'(\mathbb{Z}_2) \times U(1) \times U(1), \quad (\text{A4})$$

where $D'(\mathbb{Z}_2)$ is an Abelian theory similar to $D(\mathbb{Z}_2)$, the quantum double of \mathbb{Z}_2 (a.k.a. the toric code). The two $U(1)$ factors describe the charge and spin of the particles. Its data is listed in Ref. 79 and also as $\nu = 8$ in Table 2 of Ref. 81. The fundamental quasiholes of this state carrying Fib topological charge τ , and electric charge of either $e/7$ or $2e/7$.

As these theories are the direct product of a Fibonacci theory with Abelian sectors, the braiding statistics of quasiparticle excitations carrying the non-trivial Fibonacci charge are computationally universal.

Appendix B: Limiting the number of particles

In this Appendix, we will provide some details on how we can restrict the quasiparticle spectrum to just two quasiparticles, namely the trivial “vacuum” quasiparticle I , and a “fundamental” or “elementary” excitation. This excitation has the smallest possible electric charge, and is fundamental in the sense that all other excitations can be obtained from it by repeated fusion. The reason behind this truncation is to come up with a model which is tractable, because the Hilbert space grows exponentially in the number of quasiparticle types. Apart from the truncation of the spectrum to two quasiparticle types only, we also need that the energy associated with these particles is the same. To achieve both goals, one has two tools, in principle. In particular, one can consider using a gate which couples linearly to the charge, or consider the charging energy associated with localizing the anyons on quantum dots. As we will show below, by using a gate alone, one can arrange the system to have degenerate levels for the quasiparticles, but it turns out that this lead to a degeneracy larger than two. To split this degeneracy, the quantum dot charging is essential.

After we explain how we can restrict the number of quasiparticles to these two types, we explain how we can map the obtained model to the anyonic models introduced in Ref. 54 (in the case $\rho = 1$). We do not consider the MR and $k = 3$ RR cases separately, but directly consider the general case of the fermionic RR states for arbitrary k (which includes MR at $k = 2$). In addition, we only focus on those aspects which we will need for our purposes in this paper.

We start by decomposing the operators creating the different types of particles into two pieces, one associated with the non-Abelian statistics, the other with the electric charge of the quasiparticles. The operator describing the fundamental quasiparticles, which have charge $e/(k+2)$ is of the form $\Phi_1^1 e^{i\varphi/(\sqrt{k(k+2)})}$, where Φ_1^1 is a parafermion field, corresponding to σ and σ_1 for $k = 2$

and $k = 3$, respectively, using the notation of section II B.

The vertex operator $e^{i\varphi/(\sqrt{k(k+2)})}$, where φ is a chiral bosonic scalar field, gives the charge of the quasiparticle.

The energy of the quasiparticles in a finite geometry (such as the quantum dots used to localize the quasiparticles) are proportional to the scaling dimensions of the fields creating the particles. For each possible charge of the quasiparticles, $m\frac{e}{k+2}$, with $m = 0, 1, \dots, k$, we only consider the particles with the lowest scaling dimension.

These are given by $\Phi_m^m e^{im\varphi/(\sqrt{k(k+2)})}$. There are two contributions to the scaling dimension: the parafermion field Φ_m^m contributes $\Delta_{\Phi_m^m} = \frac{m(k-m)}{k(k+2)}$ and the charge sector contributes $\Delta_\phi(m) = \frac{m^2}{k(k+2)}$, giving a total scaling dimension $\Delta_j = \frac{m}{(k+2)}$, which is therefore proportional to the charge of the excitations.

We would like to create a situation in which we have one non-trivial quasiparticle that is degenerate with the vacuum, and an appreciable gap to the other types of quasiparticle excitations. The first thing we could try to do is to lower the energy of the charge $e/(k+2)$ fundamental quasiparticle by means of an added potential, such that it becomes degenerate with the vacuum. However, we just saw that adding such a potential will actually create a set of $k+1$ degenerate states. To circumvent this problem, we will assume that, in addition to such a potential, there is also a charging energy proportional to q^2 , where q is the charge of the excitation. Effectively, this modifies the amplitude of the quadratic contribution to the scaling dimension, coming from the charge part⁴⁸. Thus, by adding the charging energy, and the energy associated with a suitable potential, we indeed can create the situation of two degenerate lowest lying states (one being the vacuum), separated from the others by a gap.

We have just argued that we can consider a chain of itinerant anyons, consisting of vacancies with quantum numbers $(I, 0)$ and fundamental quasiparticle excitations with quantum numbers $(\Phi_1^1, e/(k+2))$. Under fusion, the electric charge is merely additive, and we will therefore concentrate on the non-Abelian sector only. In the original anyonic chain models, the constituent anyons belong to the pure $SU(2)_k$ theory. The anyonic systems we study can be mapped to these by noting that the Φ_1^1 parafermionic field carries spin $j = 1/2$ $SU(2)_k$ topological charge, together with some Abelian topological charges.

-
- * didier.poilblanc@irsamc.ups-tlse.fr
- ¹ J. M. Leinaas and J. Myrheim, *Nuovo Cimento B* **37B**, 1 (1977).
 - ² G. A. Goldin, R. Menikoff, and D. H. Sharp, *Phys. Rev. Lett.* **54**, 603 (1985).
 - ³ K. Fredenhagen, K. H. Rehren, and B. Schroer, *Commun. Math. Phys.* **125**, 201 (1989).
 - ⁴ J. Fröhlich and F. Gabbiani, *Rev. Math. Phys.* **2**, 251 (1990).
 - ⁵ G. Moore and N. Read, *Nucl. Phys. B* **360**, 362 (1991).
 - ⁶ N. Read and E. Rezayi, *Phys. Rev. B* **59**, 8084 (1999), [cond-mat/9809384](#).
 - ⁷ S.-S. Lee, S. Ryu, C. Nayak, and M. P. A. Fisher, *Phys. Rev. Lett.* **99**, 236807 (2007), [arXiv:0707.0478](#).
 - ⁸ M. Levin, B. I. Halperin, and B. Rosenow, *Phys. Rev. Lett.* **99**, 236806 (2007), [arXiv:0707.0483](#).
 - ⁹ P. Bonderson and J. K. Slingerland, *Phys. Rev. B* **78**, 125323 (2008), [arXiv:0711.3204](#).
 - ¹⁰ I. P. Radu, J. B. Miller, C. M. Marcus, M. A. Kastner, L. N. Pfeiffer, and K. W. West, *Science* **320**, 899 (2008), [arXiv:0803.3530](#).
 - ¹¹ R. L. Willett, L. N. Pfeiffer, and K. W. West, *Proc. Natl. Acad. Sci.* **106**, 8853 (2009), [arXiv:0807.0221](#).
 - ¹² R. L. Willett, L. N. Pfeiffer, and K. W. West (2012), [arXiv:1204.1993](#).
 - ¹³ R. Willett, J. P. Eisenstein, H. L. Stormer, D. C. Tsui, A. C. Gossard, and J. H. English, *Phys. Rev. Lett.* **59**, 1776 (1987).
 - ¹⁴ W. Pan, J.-S. Xia, V. Shvarts, D. E. Adams, H. L. Stormer, D. C. Tsui, L. N. Pfeiffer, K. W. Baldwin, and K. W. West, *Phys. Rev. Lett.* **83**, 3530 (1999), [cond-mat/9907356](#).
 - ¹⁵ J. P. Eisenstein, K. B. Cooper, L. N. Pfeiffer, and K. W. West, *Phys. Rev. Lett.* **88**, 076801 (2002), [cond-mat/0110477](#).
 - ¹⁶ J. S. Xia, W. Pan, C. L. Vicente, E. D. Adams, N. S. Sullivan, H. L. Stormer, D. C. Tsui, L. N. Pfeiffer, K. W. Baldwin, and K. W. West, *Phys. Rev. Lett.* **93**, 176809 (2004), [cond-mat/0406724](#).
 - ¹⁷ A. Kumar, G. A. Csáthy, M. J. Manfra, L. N. Pfeiffer, and K. W. West, *Phys. Rev. Lett.* **105**, 246808 (2010), [arXiv:1009.0237](#).
 - ¹⁸ P. Bonderson, A. E. Feiguin, G. Moller, and J. K. Slingerland, *Phys. Rev. Lett.* **108**, 036806 (2012), [arXiv:0901.4965](#).
 - ¹⁹ M. Hermanns, *Phys. Rev. Lett.* **104**, 056803 (2010), [arXiv:0906.2073](#).
 - ²⁰ E. Ardonne and K. Schoutens, *Phys. Rev. Lett.* **82**, 5096 (1999), [cond-mat/9811352](#).
 - ²¹ G. E. Volovik, *Soviet Journal of Experimental and Theoretical Physics Letters* **70**, 792 (1999), [cond-mat/9911374](#).
 - ²² N. Read and D. Green, *Phys. Rev. B* **61**, 10267 (2000), [cond-mat/9906453](#).
 - ²³ A. Y. Kitaev, *Physics-Uspekhi* **44**, 131 (2001), [cond-mat/0010440](#).
 - ²⁴ L. Fu and C. Kane, *Phys. Rev. Lett.* **100**, 096407 (2008), [arXiv:0707.1692](#).
 - ²⁵ J. Sau, R. Lutchyn, S. Tewari, and S. D. Sarma, *Phys. Rev. Lett.* **104**, 040502 (2010), [arXiv:0907.2239](#).
 - ²⁶ J. Alicea, *Phys. Rev. B* **81**, 125318 (2010), [arXiv:0912.2115](#).
 - ²⁷ R. M. Lutchyn, J. D. Sau, and S. Das Sarma, *Phys. Rev. Lett.* **105**, 077001 (2010), [arXiv:1002.4033](#).
 - ²⁸ Y. Oreg, G. Refael, and F. von Oppen (2010), [arXiv:1003.1145](#).
 - ²⁹ J. Alicea, *Rep. Prog. Phys.* **75**, 076501 (2012), [arXiv:1202.1293](#).
 - ³⁰ V. Mourik, K. Zuo, S. Frolov, S. Plissard, E. Bakkers, and L. Kouwenhoven, *Science* **336**, 1003 (2012), [arXiv:1204.2792](#).
 - ³¹ L. P. Rokhinson, X. Liu, and J. K. Furdyna (2012), [arXiv:1204.4212](#).
 - ³² M. Deng, C. Yu, G. Huang, M. Larsson, P. Caroff, and H. Xu (2012), [arXiv:1204.4130](#).
 - ³³ A. Das, Y. Ronen, Y. Most, Y. Oreg, M. Heiblum, and H. Shtrikman (2012), [arXiv:1205.7073](#).
 - ³⁴ P. W. Anderson, *Phys. Rev.* **164**, 352 (1967).
 - ³⁵ S. Tomonaga, *Prog. Theor. Phys.* **5**, 544 (1950).
 - ³⁶ J. M. Luttinger, *J. Math. Phys.* **15**, 609 (1963).
 - ³⁷ F. D. M. Haldane, *J. Phys. C* **14**, 2585 (1981).
 - ³⁸ D. Poilblanc, M. Troyer, E. Ardonne, and P. Bonderson, *Phys. Rev. Lett.* **108**, 207201 (2012), [arXiv:1112.5950](#).
 - ³⁹ F.-C. Zhang and T. M. Rice, *Phys. Rev. B* **37**, 3759 (1988).
 - ⁴⁰ J. Hubbard, *Proc. Roy. Soc. London A* **276**, 238 (1963).
 - ⁴¹ M. C. Gutzwiller, *Phys. Rev. Lett.* **10**, 159 (1963).
 - ⁴² J. Kanamori, *Prog. of Theor. Phys. (Kyoto)* **30**, 275 (1963).
 - ⁴³ P. A. Bares and G. Blatter, *Phys. Rev. Lett.* **64**, 2567 (1990).
 - ⁴⁴ N. Kawakami and S.-K. Yang, *Phys. Rev. Lett.* **65**, 2309 (1990).
 - ⁴⁵ P.-A. Bares, G. Blatter, and M. Ogata, *Phys. Rev. B* **44**, 130 (1991).
 - ⁴⁶ M. Ogata, M. U. Luchini, S. Sorella, and F. F. Assaad, *Phys. Rev. Lett.* **66**, 2391 (1991).
 - ⁴⁷ P. Bonderson, *Phys. Rev. Lett.* **103**, 110403 (2009), [arXiv:0905.2726](#).
 - ⁴⁸ P. Bonderson, C. Nayak, and K. Shtengel, *Phys. Rev. B* **81**, 165308 (2010), [arXiv:0909.1056](#).
 - ⁴⁹ A. Stern and B. I. Halperin, *Phys. Rev. Lett.* **96**, 016802 (2006), [cond-mat/0508447](#).
 - ⁵⁰ R. Ilan, E. Grosfeld, and A. Stern, *Phys. Rev. Lett.* **100**, 086803 (2008), [arXiv:0912.4394](#).
 - ⁵¹ R. Ilan, E. Grosfeld, K. Schoutens, and A. Stern, *Phys. Rev. B* **79**, 245305 (2009), [arXiv:0803.1542](#).
 - ⁵² A. Stern, B. Rosenow, R. Ilan, and B. I. Halperin, *Phys. Rev. B* **82**, 085321 (2010), [arXiv:0912.4394](#).
 - ⁵³ A. Messiah, *Quantum Mechanics* (North-Holland, Amsterdam, 1962).
 - ⁵⁴ A. Feiguin, S. Trebst, A. W. W. Ludwig, M. Troyer, A. Kitaev, Z. Wang, and M. H. Freedman, *Phys. Rev. Lett.* **98**, 60409 (2007), [cond-mat/0612341](#).
 - ⁵⁵ G. Andrews, R. Baxter, and P. Forrester, *J. Stat. Phys.* **35**, 193 (1984).
 - ⁵⁶ M. Ogata and H. Shiba, *Phys. Rev. B* **41**, 2326 (1990).
 - ⁵⁷ H. Shiba and M. Ogata, *Int. J. Mod. Phys. B* **5**, 31 (1991).
 - ⁵⁸ A. Parola and S. Sorella, *Phys. Rev. B* **45**, 13156 (1992).
 - ⁵⁹ J. Cardy and P. Calabrese, *J. Stat. Mech.* p. P04023 (2010), [arXiv:1002.4353](#).
 - ⁶⁰ I. Affleck and A. W. W. Ludwig, *Phys. Rev. Lett.* **67**, 161 (1991).
 - ⁶¹ P. Calabrese and J. Cardy, *J. Stat. Mech.* **0406**, P06002 (2004), [hep-th/0405152](#).

- ⁶² N. Laflorencie, E. S. Sorensen, M.-S. Chang, and I. Affleck, Phys. Rev. Lett. **96**, 100603 (2006), cond-mat/0512475.
- ⁶³ G. Roux, S. Capponi, P. Lecheminant, and P. Azaria, Eur. Phys. J. B **68**, 293 (2009), arXiv:0807.0412.
- ⁶⁴ I. Affleck, N. Laflorencie, and E. S. Sorensen, J. Phys. A: Math. Theor. **42**, 504009 (2009), arXiv:0906.1809.
- ⁶⁵ D. Poilblanc, A. W. Ludwig, S. Trebst, and M. Troyer, Phys. Rev. B **83**, 134439 (2011), arXiv:1101.1186.
- ⁶⁶ N. Read and A. W. W. Ludwig, Phys. Rev. B **63**, 024404 (2000), arXiv:cond-mat/0007255.
- ⁶⁷ E. Grosfeld and A. Stern, Phys. Rev. B **73**, 201303(R) (2006), cond-mat/0511670.
- ⁶⁸ E. Grosfeld and K. Schoutens, Phys. Rev. Lett **103**, 076803 (2009), arXiv:0810.1955.
- ⁶⁹ A. W. Ludwig, D. Poilblanc, S. Trebst, and M. Troyer, New. J. Phys. **13**, 045014 (2011), arXiv:1003.3453.
- ⁷⁰ G. Moore and N. Seiberg, Commun. Math. Phys. **123**, 177 (1989).
- ⁷¹ M. H. Freedman, M. J. Larsen, and Z. Wang, Commun. Math. Phys. **228**, 177 (2002), math/0103200.
- ⁷² E. Witten, Comm. Math. Phys. **121**, 351 (1989).
- ⁷³ J. Wess and B. Zumino, Phys. Lett. B **37**, 95 (1971).
- ⁷⁴ E. Witten, Nucl. Phys. B **223**, 422 (1983).
- ⁷⁵ V. F. R. Jones, Bull. Am. Math. Soc. **12**, 103 (1985).
- ⁷⁶ M. H. Freedman, M. J. Larsen, and Z. Wang, Commun. Math. Phys. **227**, 605 (2002), quant-ph/0001108.
- ⁷⁷ A. Kirillov and N. Reshetikhin, in *Infinite dimensional Lie algebras and groups*, edited by V. G. Kac (World Scientific, Singapore, 1988), p. 285, proceedings of the conference held at CIRM, Luminy, Marseille.
- ⁷⁸ E. Ardonne and J. Slingerland, J. Phys. A **43**, 395205 (2010), arXiv:1004.5456.
- ⁷⁹ P. H. Bonderson, Ph.D. thesis (2007).
- ⁸⁰ P. Bonderson, K. Shtengel, and J. K. Slingerland, Annals of Physics **323**, 2709 (2008), arXiv:0707.4206.
- ⁸¹ A. Kitaev, Annals Phys. **321**, 2 (2006), cond-mat/0506438.
- ⁸² S. Trebst, M. Troyer, Z. Wang, and A. W. W. Ludwig, Prog. Theor. Phys. Supp. **176**, 384 (2008), arXiv:0902.3275.
- ⁸³ The Ising TQFT has the same fusion algebra as $SU(2)_2$, but the σ and $j = \frac{1}{2}$ anyons have different scaling dimensions ($h_\sigma = 1/16$ and $h_{\frac{1}{2}} = 3/16$, respectively). The scaling dimensions of the ψ and $j = 1$ anyons are identical, $h_\psi = h_1 = 1/2$.
- ⁸⁴ For k odd, the restriction to the integer-valued topological charge (generalized angular momentum) can be made by using the map obtained by fusing with the topological charge $j = \frac{k}{2}$, namely $j \times \frac{k}{2} = \frac{k}{2} - j$, which for $k = 3$ maps $\frac{1}{2} \leftrightarrow 1$ and $\frac{3}{2} \leftrightarrow 0$. For more details, we refer to Refs. [79,82](#).
- ⁸⁵ For the bosonic states, the particle identified with the vacuum is a boson. In the fermionic case, one cannot simply identify the electron with the vacuum, because it is a fermion, which obviously has different braiding statistics than the vacuum (which is a boson). Considering fusion and braiding, one could instead simply identify pairs of electrons with vacuum. However, the resulting theory will not be modular, meaning the S-matrix is degenerate. This poses a problem when one wishes to define the theory on arbitrary surfaces, including the torus. A solution is to put each charge into a Z_2 doublet, e.g. the vacuum and electron form the vacuum doublet, and every charge together with the charge obtained by fusion with an electron form a doublet. Then the S-matrix of doublets is modular. In practice, one can take the fusion rules assuming identification of electron with vacuum.